Medical Ultrasonic Imaging

Problem Presenter

Bruno Haider
GE Global Research Center

Problem Participants

Dean Duffy, NASA/Goddard
David A. Edwards, University of Delaware
Brian Emmanuel, New Jersey Institute of Technology
Kim Fessel, Rensselær Polytechnic Institute
Linghong Hu, Rensselær Polytechnic Institute
Rich Moore, New Jersey Institute of Technology
Colin Please, University of Southampton
Don Schwendeman, Rensselær Polytechnic Institute
Susie Seal, Arizona State University
Yunfei Song, SUNY Buffalo
He Yang, Rensselær Polytechnic Institute
and others...

Twenty-Sixth Annual Workshop on Mathematical Problems in Industry
June 14–18, 2010
Rensselær Polytechnic Institute

Section 1: Introduction

Medical ultrasound devices are used extensively to "see" soft tissue structures inside the body. High-amplitude ultrasound waves are sent from a transducer into the tissue. The resulting reflected waves are collected by the same transducer, and then converted into an electrical signal. This signal is then processed to produce a visual image of the scanned tissue.

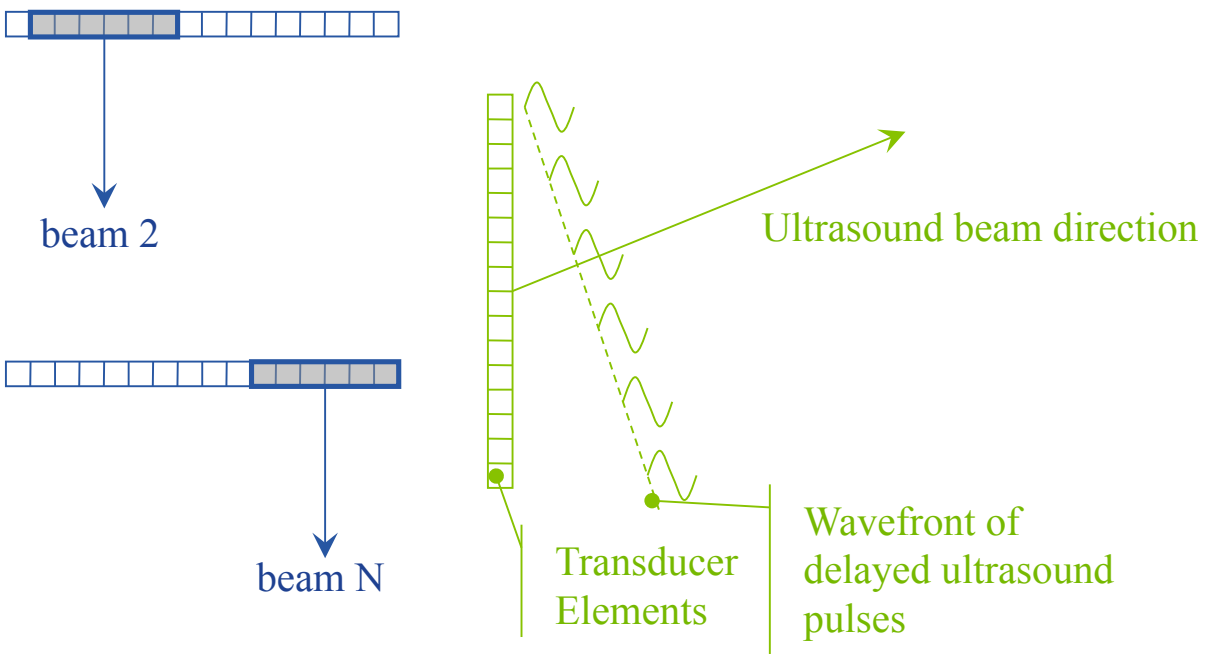

Figure 1.1. Schematic of transducer array.

A schematic of a transducer is shown in Fig. 1.1. Each transducer is made up of a series of transducer *elements*. A subset of these elements sends out waves either at the same time to produce a linear (plane) wave profile or asynchronously to produce a wave at a given angle from the device (used for wedge scans).

Each transducer element is made up of three parts, as shown in Fig. 1.2. A piezoelectric substance (PZT) converts electric impulses to pressure waves and vice versa. As it compresses in the $\tilde{x}$-direction, (which points normal to the transducer/skin interface), it expands in the $\tilde{y}$-direction (parallel to the interface), as shown in Fig. 1.3, where $\tilde{x}$ points up. Hence nearby elements are usually fired together.

Two *matching layers* are placed in series above the PZT. The purpose of these are to gradually step down the impedance Z from the high value in the PZT to the lower value in the tissue in order to improve imaging.

Though the media in the matching layers behaves linearly, the interface between them introduces reflections into the outgoing signal, a phenomenon known as *ringdown*.

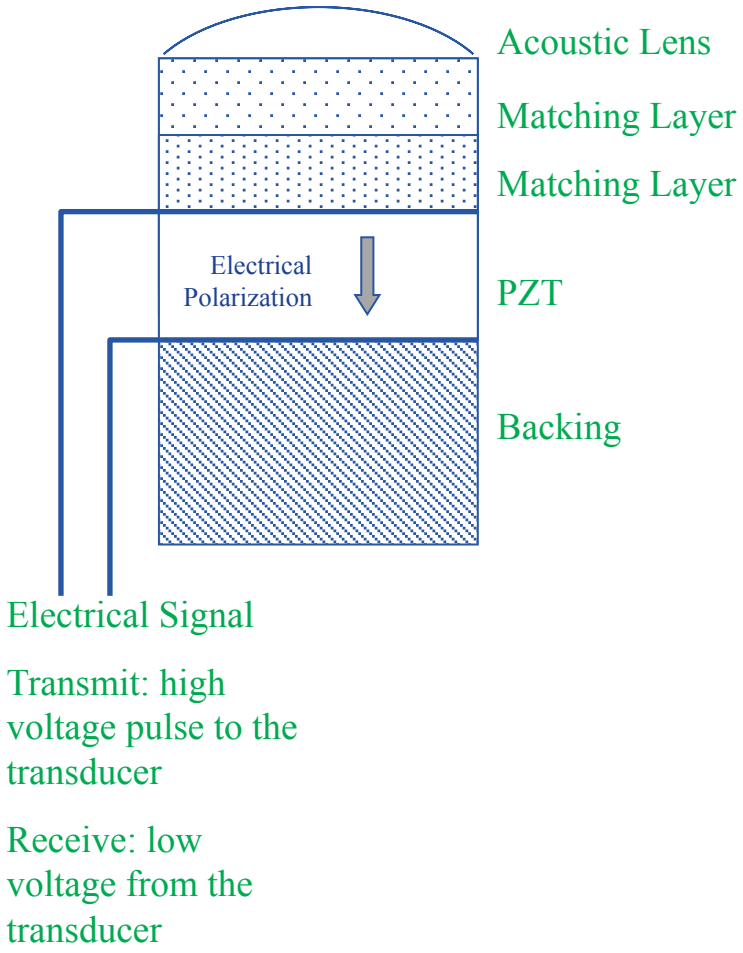

Figure 1.2. Schematic of transducer element.

This mixed wave then penetrates into the tissue, which is a nonlinear medium. The outgoing wave has a large enough amplitude that nonlinear effects are important, though the reflected waves traveling back to the transducer are small enough that a linear analysis is sufficient.

These nonlinear effects make it difficult to discern the true features of the tissue, and compensating for them is the major thrust of this investigation.

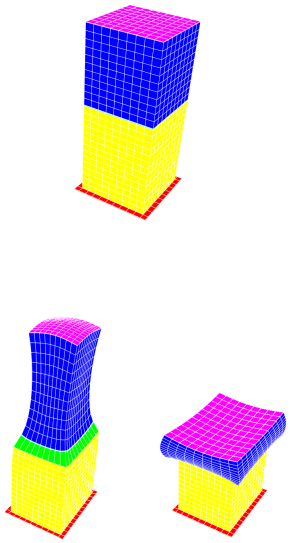

Figure 1.3. Transverse motion of PZT.

Section 2: Linear One-Layer Model, Outgoing Wave

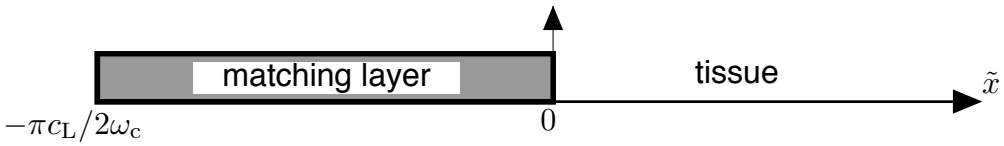

Figure 2.1. Semi-infinite one-layer model.

As a first attempt, we consider a single transducer element with only one matching layer, as shown in Fig. 2.1. (We choose the element-tissue interface to be $\tilde{x} = 0$ for algebraic convenience.) Typically in these experiments the PZT waves are modulated sine waves with characteristic frequency ω_{c}. For purposes that will be explained below, the width of the matching layer is set to be 1/4 of the wavelength of the corresponding wave, so we have

$$-\frac{2\pi c_{\mathrm{L}}}{4\omega_{\mathrm{c}}} = -\frac{\pi c_{\mathrm{L}}}{2\omega_{\mathrm{c}}} \le \tilde{x} \le 0, \tag{2.1}$$

where c_{L} is the wave speed in the layer.

Typically the distance between the structures of interest and the transducer is much larger than the layer width (see Appendix). This means that though there may be internal reflection in the matching layers, their primary effect is to contaminate the signal when the transducer is set to "listening mode". Hence for the purposes of this model we take the tissue to be semi-infinite, and determine the signal at some arbitrary distance from the PZT as a function of time.

Moreover we assume linear behavior for the tissue, so the governing equations for the pressure displacement $\tilde{p}$ are as follows:

$$\frac{\partial^2 \tilde{p}_{\mathrm{L}}}{\partial \tilde{t}^2} = c_{\mathrm{L}}^2 \frac{\partial^2 \tilde{p}_{\mathrm{L}}}{\partial \tilde{x}^2}, \qquad -\frac{\pi c_{\mathrm{L}}}{2\omega_{\mathrm{c}}} \le \tilde{x} \le 0, \tag{2.2a}$$

$$\frac{\partial^2 \tilde{p}_{\mathrm{T}}}{\partial \tilde{t}^2} = c_{\mathrm{T}}^2 \frac{\partial^2 \tilde{p}_{\mathrm{T}}}{\partial \tilde{x}^2}, \qquad \tilde{x} \ge 0, \tag{2.2b}$$

where the subscript "T" refers to "tissue". The pressure boundary condition is given by the PZT wave

$$\tilde{p}\left(-\frac{\pi c_{\mathrm{L}}}{2\omega_{\mathrm{c}}}, \tilde{t}\right) = p_{\mathrm{c}} p_{\mathrm{P}}(\tilde{t}), \quad \tilde{t} > 0, \tag{2.3}$$

where p_{c} is some characteristic value of the displacement and the subscript "P" refers to "PZT". Here the (obvious) restriction on $\tilde{t}$ will become important later.

Equations (2.2) and (2.3) motivate the following scalings:

$$p(x,t) = \frac{\tilde{p}(\tilde{x},\tilde{t})}{p_{\mathrm{c}}}, \qquad x = \frac{\omega_{\mathrm{c}}\tilde{x}}{c_{\mathrm{L}}}, \qquad t = \omega_{\mathrm{c}}\tilde{t}. \tag{2.4}$$

Substituting (2.4) into (2.2) and (2.3), we obtain the following dimensionless system:

$$p_{\mathrm{c}}\omega_{\mathrm{c}}^2\frac{\partial^2 p_{\mathrm{L}}}{\partial t^2} = c_{\mathrm{L}}^2\frac{p_{\mathrm{c}}\omega_{\mathrm{c}}^2}{c_{\mathrm{L}}^2}\frac{\partial^2 p_{\mathrm{L}}}{\partial x^2}, \qquad -\frac{\pi c_{\mathrm{L}}}{2\omega_{\mathrm{c}}}\left(\frac{\omega_{\mathrm{c}}}{c_{\mathrm{L}}}\right) \le x \le 0$$

$$\frac{\partial^2 p_{\mathrm{L}}}{\partial t^2} = \frac{\partial^2 p_{\mathrm{L}}}{\partial x^2}, \quad -\frac{\pi}{2} \le x \le 0, \tag{2.5a}$$

$$\frac{\partial^2 p_{\mathrm{T}}}{\partial t^2} = \frac{1}{r^2}\frac{\partial^2 p_{\mathrm{T}}}{\partial x^2}, \quad x \ge 0, \qquad r = \frac{c_{\mathrm{L}}}{c_{\mathrm{T}}}, \tag{2.5b}$$

$$u(-\pi/2, t) = p_{\mathrm{P}}(t), \quad t > 0. \tag{2.6}$$

Note that r is the *inverse* of the sound speed ratio; we use it for later algebraic simplicity. Note also from the Appendix that $r > 1$.

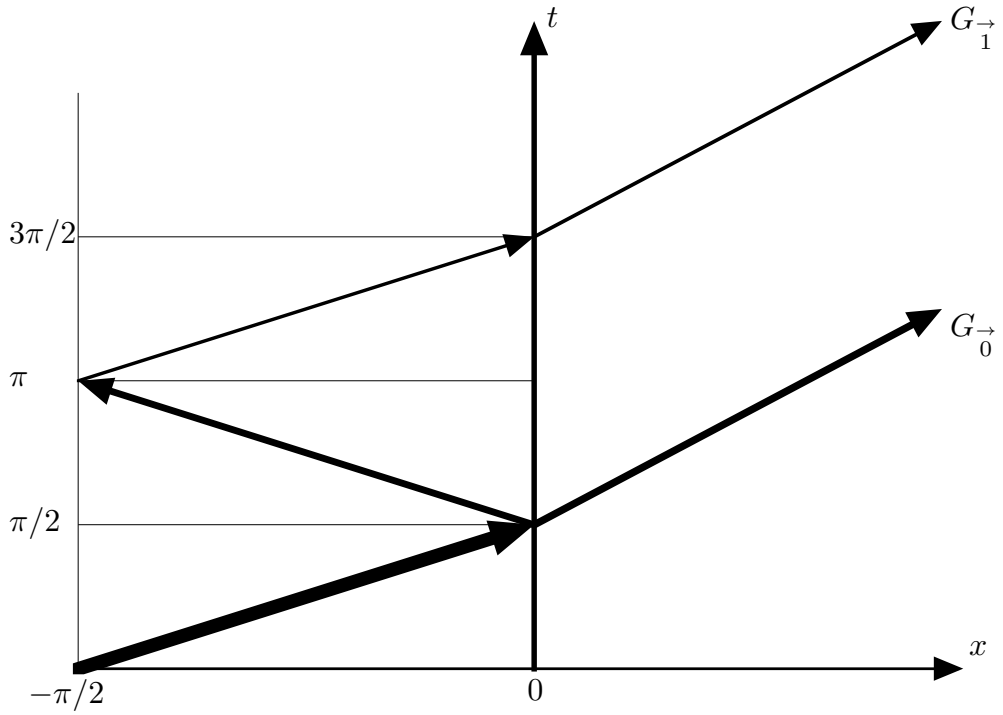

Figure 2.2. Characteristic diagram for Green's function, outgoing wave.

To solve the problem for general $p_{\mathrm{P}}(t)$, we first construct the Green's function $G(x,t)$ for the problem by solving for $p_{\mathrm{P}}(t) = \delta(t)$. This solution can be constructed using the method of characteristics, as illustrated in Fig. 2.2. We note from (2.5a) that the normalized sound speed in the layer is 1. Hence we have the following solutions for $0 < t < \pi/2$:

$$G_{\mathrm{L}}(x,t) = \delta(t - (x + \pi/2)), \quad 0 < t < \pi/2, \tag{2.7a}$$

$$G_{\mathrm{T}}(x,t) = 0, \quad 0 < t - rx < \frac{\pi}{2}. \tag{2.7b}$$

Note from (2.7b) that the range before which the first pulse hits increases with increasing x, as it takes the wave (traveling with speed r^{-1}) longer to reach there. Since r^{-1}, the sound speed ratio, is less than 1, we have the characteristic bending shown in Fig. 2.2.

At time $t = \pi/2$, the wave hits the boundary between layer and tissue. The discontinuity causes the creation of a transmitted wave and a reflected wave. The (amplitude) reflection coefficient R_{T} is defined as

$$R_{\mathrm{T}} = \frac{Z_{\mathrm{T}} - Z_{\mathrm{L}}}{Z_{\mathrm{T}} + Z_1}. \tag{2.8}$$

Note from the values in the Appendix that in this case, $-1 < R_{\mathrm{T}} < 0$. Since we are using the amplitude reflection coefficient, this means that the amplitude transmission coefficient is just $1 - R_{\mathrm{T}}$. So the amplitude increases in the tissue because the signal impedance is smaller there. (When perusing the literature, one must take care to distinguish between the amplitude reflection coefficient and the energy reflection coefficient, which is R_{T}^2 in our notation.)

Since the amplitude of our initial wave is 1, this implies that

$$G_{\mathrm{T}}(x,t) = (1 - R_{\mathrm{T}})\delta\left(t - \frac{\pi}{2} - rx\right), \quad \frac{\pi}{2} < t - rx < 3\pi/2. \tag{2.9}$$

where the value of the upper limit on t will be established later. The reflected wave in the layer now moves with speed -1 until it impinges upon the PZT boundary, so we have

$$G_{\mathrm{L}}(x,t) = R_{\mathrm{T}}\delta\left(t + (x - \pi/2)\right), \quad \pi/2 < t < \pi. \tag{2.10}$$

Note that the form of the phase shift can be seen by the method of images.

This reflected wave reflects again from the PZT boundary. Here the reflection coefficient is given by R_{P}, which is greater than zero because the layer adjoining the PZT is more rigid. Hence we have

$$G_{\mathrm{L}}(x,t) = R_{\mathrm{P}}R_{\mathrm{T}}\delta((t - \pi) - (x + \pi/2)), \quad \pi < t < 3\pi/2. \tag{2.11}$$

But this is just the expression for G_{L} in (2.7a), scaled down by R_{T} and phase shifted by π. Hence by the shift of (2.7) we have that there is no additional wave in the tissue until $t = 3\pi/2$, at which point we have an additional "echo" of the initial signal of the form in (2.9), scaled down by R_{T} and shifted by π, so we have

$$G_{\mathrm{T}}(x,t) = (1 - R_{\mathrm{T}})\left[\delta\left(t - \frac{\pi}{2} - rx\right) + R_{\mathrm{P}}R_{\mathrm{T}}\delta\left((t - \pi) - \frac{\pi}{2} - rx\right)\right], \quad \frac{3\pi}{2} < t - rx < \frac{5\pi}{2}. \tag{2.12}$$

We introduce the following notation:

$$G_{\underset{j}{\rightarrow}}(x,t) = (1 - R_{\mathrm{T}})(R_{\mathrm{P}}R_{\mathrm{T}})^j\delta\left((t - j\pi) - \frac{\pi}{2} - rx\right). \tag{2.13}$$

$G_{\underset{j}{\rightarrow}}$ is just the jth echo from the main signal, and the arrow to the right indicates that these are echoes of an outgoing wave. Here the first term represents the gain by moving from PZT into the tissue. The $(R_{\mathrm{P}}R_{\mathrm{T}})^j$ represents the decay in signal for each reflection

that occurs inside the PZT. Each reflection takes $t = \pi$ (see Fig. 2.2), which accounts for the $j\pi$ phase shift in the δ-function.

Then (2.12) becomes

$$G_{\mathrm{T}}(x,t) = \sum_{j=0}^{1} G_{\underset{j}{\rightarrow}}(x,t), \qquad \frac{(2+1)\pi}{2} < t - rx < \frac{(2+3)\pi}{2}. \tag{2.14}$$

But the echoing process continues forever, and hence we have

$$G_{\mathrm{T}}(x,t) = \sum_{j=0}^{J} G_{\underset{j}{\rightarrow}}(x,t), \qquad t - rx \in \left[\frac{(2J+1)\pi}{2}, \frac{(2J+3)\pi}{2}\right]. \tag{2.15}$$

Hence at some position $x = \ell$, the signal is just a series of pulses arriving $t = \pi$ apart, each one smaller in magnitude than the last. Hence J is simply the number of echoes that have had time to reach position x, and j indexes the echoes. But since the δ function is zero for nonzero argument, we don't need the restriction on t, and we may write

$$G_{\mathrm{T}}(x,t) = \sum_{j=0}^{\infty} G_{\underset{j}{\rightarrow}}(x,t) \tag{2.16}$$

for all t. This form is useful for later calculations, but for most purposes, we will stick with the finite form (2.15).

We also remark that if we relax the assumption that there is total reflection at the PZT interface, but treat the PZT as semi-infinite (so there are no reflections from the back of the PZT), we may simply redefine our reflection coefficient to take into account that reflection. (We shall do this in the next section.) Treating the PZT as finite introduces more reflections that are beyond the scope of this section.

Given G_{T}, the signal in the tissue for an arbitrary boundary condition is given by

$$\begin{aligned} p_{\mathrm{T}}(x,t) &= \int_0^t p_{\mathrm{P}}(\tau) G_{\mathrm{T}}(x, t-\tau)\, d\tau \\ &= (1 - R_{\mathrm{T}}) \sum_{j=0}^{J} (R_{\mathrm{P}} R_{\mathrm{T}})^j \int_0^t p_{\mathrm{P}}(\tau) \delta\left((t - \tau - j\pi) - \frac{\pi}{2} - rx\right) d\tau. \\ &= \sum_{j=0}^{J} p_{\underset{j}{\rightarrow}}(x,t), \qquad t - rx \in \left[\frac{(2J+1)\pi}{2}, \frac{(2J+3)\pi}{2}\right], \end{aligned} \tag{2.17a}$$

$$p_{\underset{j}{\rightarrow}}(x,t) = (1 - R_{\mathrm{T}})(R_{\mathrm{P}} R_{\mathrm{T}})^j p_{\mathrm{P}}\left((t - j\pi) - \frac{\pi}{2} - rx\right). \tag{2.17b}$$

Since reflections arrive at intervals of π, any wave boundary condition with period greater than π will have overlap between the initial signal and the first reflection, as shown in Fig. 2.3.

In reality, we will not have p_{T} everywhere, but at some point ℓ (where we may have placed a hydrophone) and at discrete times when the data is sampled. Obviously no signal can be heard until

$$\frac{\pi}{2} + \ell r,$$

so that would be the first time sampled. Sampling rates are expressed in terms of frequency f_{s}. To convert them into dimensionless time, we have

$$t_{\mathrm{s}} = \frac{\omega_{\mathrm{c}}}{f_{\mathrm{s}}} = \pi \frac{2f_{\mathrm{c}}}{f_{\mathrm{s}}}. \tag{2.18}$$

It would be best if the same points could be used over and over again, which corresponds to them being spaced like $t_{\mathrm{s}} = \pi/M$, for some integer M. This is not quite true for the frequency ratio in the Appendix.

Using this discussion, we define the sampling times by

$$t_m = \frac{m\pi}{M} + \frac{\pi}{2} + \ell r. \tag{2.19}$$

We now substitute (2.19) into (2.17a). Because of the finite nature of the problem, it is more useful to return back to the finite representation in (2.17a). Doing so, we have

$$\begin{aligned}
p_{\mathrm{T}}(\ell, t_m) &= \sum_{j=0}^{J} p_{\underset{j}{\rightarrow}} \left(\ell, \frac{m\pi}{M} + \frac{\pi}{2} + \ell r\right) \\
&= (1 - R_{\mathrm{T}}) \sum_{j=0}^{J} (R_{\mathrm{P}} R_{\mathrm{T}})^j p_{\mathrm{P}} \left(\frac{m\pi}{M} - j\pi\right), \quad \frac{m\pi}{M} + \frac{\pi}{2} \in \left[\frac{(2J+1)\pi}{2}, \frac{(2J+3)\pi}{2}\right] \\
&= (1 - R_{\mathrm{T}}) \sum_{j=0}^{J} (R_{\mathrm{P}} R_{\mathrm{T}})^j p_{\mathrm{P}} \left(\frac{(m - Mj)\pi}{M}\right) \\
p_m &= (1 - R_{\mathrm{T}}) \sum_{j=0}^{J} (R_{\mathrm{P}} R_{\mathrm{T}})^j q_{m-Mj}, \quad m \in [MJ, M(J+1)], \qquad (2.20\mathrm{a}) \\
p_m &= p_{\mathrm{T}}(\ell, t_m), \qquad q_m = p_{\mathrm{P}} \left(\frac{m\pi}{M}\right). \qquad (2.20\mathrm{b})
\end{aligned}$$

But (2.20a) is a set of linear equations in the variables p_m and q_m, and so can be written schematically as

$$\mathbf{p} = C\mathbf{q},$$

where the bold notation means the vectors of the corresponding samples, and C is some matrix. So to obtain the initial signal is equivalent to computing

$$\mathbf{q} = C^{-1}\mathbf{p}.$$

Note that C is a function of the material.

We now consider the case of a single mode:

$$p_{\mathrm{P}}(t) = \hat{p}_{\mathrm{P}}(\omega)e^{i\omega t}, \tag{2.21}$$

which has the desirable property that

$$\begin{aligned} p_{\underset{j}{\rightarrow}}(x,t) &= \hat{p}_{\mathrm{P}}(\omega)(1-R_{\mathrm{T}})(R_{\mathrm{P}}R_{\mathrm{T}})^j \exp\left(i\omega\left(t - \frac{(2j+1)\pi}{2} - rx\right)\right) \\ &= p_{\underset{0}{\rightarrow}}(x,t)R_{\mathrm{P}}^j R_{\mathrm{T}}^j e^{-\pi i\omega j}, \\ p_{\underset{0}{\rightarrow}}(x,t) &= \hat{p}_{\mathrm{P}}(\omega)(1-R_{\mathrm{T}})\exp\left(i\omega\left(t - \frac{\pi}{2} - rx\right)\right), \end{aligned} \tag{2.22a}$$

$$\begin{aligned} p_{\mathrm{T}}(x,t) &= p_{\underset{0}{\rightarrow}}(x,t)\sum_{j=0}^{J}(R_{\mathrm{P}}R_{\mathrm{T}}e^{-\pi i\omega})^j \\ &= p_{\underset{0}{\rightarrow}}(x,t)\frac{1-\left(R_{\mathrm{P}}R_{\mathrm{T}}e^{-\pi i\omega}\right)^{J+1}}{1-R_{\mathrm{P}}R_{\mathrm{T}}e^{-\pi i\omega}}, \quad t-rx \in \left[\frac{(2J+1)\pi}{2}, \frac{(2J+3)\pi}{2}\right]. \end{aligned} \tag{2.22b}$$

Hence in this simple case the sum collapses and the expression can be written explictly. Moreover, since $|R_{\mathrm{T}}|$ and $|R_{\mathrm{P}}|$ are both less than 1, we have that

$$p_{\mathrm{T}}(x,t) \sim \frac{p_{\underset{0}{\rightarrow}}(x,t)}{1-R_{\mathrm{P}}R_{\mathrm{T}}e^{-\pi i\omega}}, \quad t \to \infty. \tag{2.23}$$

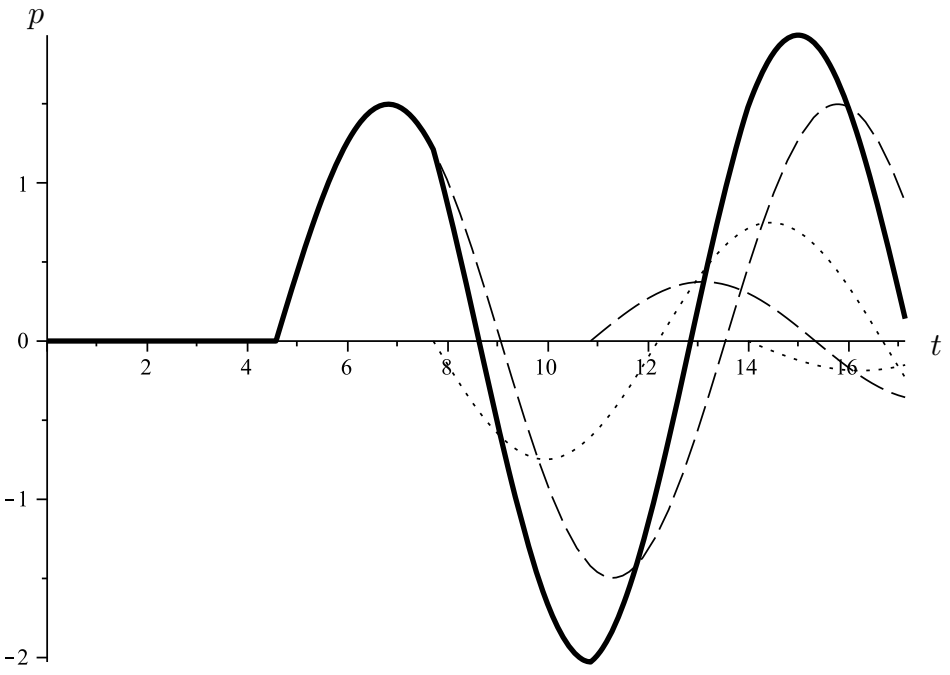

Figure 2.3. Graph of (2.22b) for $R_{\mathrm{P}} = 1$, $R_{\mathrm{T}} = -0.5$, $\omega = 0.7$, $x = 3/r$, $\hat{p}(0.7) = 1$, $n \in [0,3]$. Dark line: received signal p_{T}. Dotted/dashed lines: individual pulse echoes $p_{\underset{j}{\rightarrow}}$.

Figure 2.3 shows a graph of the solution in (2.22b) for the parameters described. Here $\omega < 1$, so the period is longer than π. Hence the initial waveform (shown by the first appearing dashed line) is not fully formed before the first echo (shown by the first appearing dotted line) distorts it. However, since this is a purely linear problem, existing filters can determine the initial waveform from the contaminated signal.

Because of the normalization used in (2.4), we know that choosing $\omega \in \mathcal{Z}$ corresponds to some multiple of the characteristic wavelength ω_{c}. In particular, choosing $\omega = 2$ yields

$$\begin{aligned} p_{\mathrm{T}}(x,t) &= p_{\underset{0}{\rightarrow}}(x,t)\frac{1-(R_{\mathrm{P}}R_{\mathrm{T}})^{J+1}}{1-R_{\mathrm{T}}} \\ &= \hat{p}_{\mathrm{P}}(2)[1-(R_{\mathrm{P}}R_{\mathrm{T}})^{J+1}]\exp\left(2i\left(t-\frac{\pi}{2}-rx\right)\right), \\ &\qquad t-rx \in \left[\frac{(2J+1)\pi}{2}, \frac{(2J+3)\pi}{2}\right], \end{aligned} \tag{2.24a}$$

$$p_{\mathrm{T}}(x,t) \sim \hat{p}_{\mathrm{P}}(2)\exp\left(2i\left(t-\frac{\pi}{2}-rx\right)\right), \quad t\to\infty, \tag{2.24b}$$

and the original waveform is reconstructed from the reflections as $t \to \infty$. Hence the choice of width as compared to a typical wavelength.

Obviously the true signal is made up of waves of varying wavelengths, and hence this nice fidelity of signal is not preserved. In particular, we note that any PZT waveform p_{p} may be expressed in terms of its Fourier transform:

$$\mathcal{F}\{p_{\mathrm{P}}(t)\} \equiv \hat{p}_{\mathrm{P}}(\omega) = \frac{1}{2\pi}\int_{-\infty}^{\infty} p_{\mathrm{P}}(t)e^{-i\omega t}\,dt, \qquad p_{\mathrm{P}}(t) = \int_{-\infty}^{\infty}\hat{p}_{\mathrm{P}}(\omega)e^{i\omega t}\,d\omega. \tag{2.25}$$

Then using the result for a single mode in (2.25), we obtain

$$\begin{aligned} p_{\mathrm{T}}(x,t) &= (1-R_{\mathrm{T}})\int_{-\infty}^{\infty}\hat{p}_{\mathrm{P}}(\omega)\frac{1-\left(R_{\mathrm{P}}R_{\mathrm{T}}e^{-\pi i\omega}\right)^{J+1}}{1-R_{\mathrm{P}}R_{\mathrm{T}}e^{-\pi i\omega}}\exp\left(i\omega\left(t-\frac{\pi}{2}-rx\right)\right)d\omega, \\ &\qquad t-rx \in \left[\frac{(2J+1)\pi}{2}, \frac{(2J+3)\pi}{2}\right], \end{aligned} \tag{2.26}$$

which describes the relationship between p_{T} and p_{P} for any boundary condition.

Section 3: Ringing Analysis

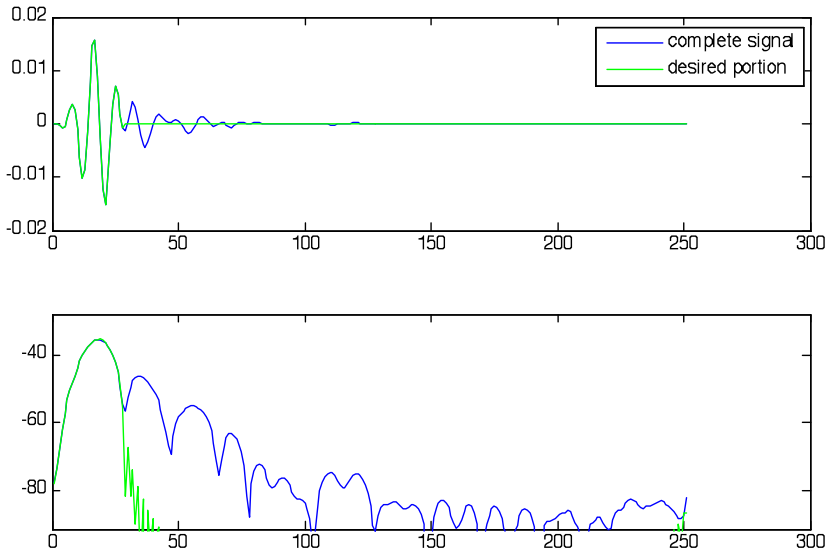

Figure 3.1. Top: typical data for received signal $p_{\mathrm{R}}(t)$. Bottom: envelope on dB ($10\log_{10}$) scale. Abscissa is measured in ticks.

A typical experimental setup occurs when the transducer is placed in a tank of water, 1.5 cm away from a steel reflector. Small-amplitude vibrations are induced in a pulse to eliminate nonlinear effects. Then the reflected waves are measured, as shown in the top graph in Fig. 3.1. As discussed previously, the data is sampled at a frequency rate f_{s}, or at a dimensional time of f_{s}^{-1}. In the experimental setup, the data is sampled at 33 MHz, which means once every

$$\frac{1}{33\times 10^6\ \mathrm{s}^{-1}} = 3.03\times 10^{-8}\ \mathrm{s}.$$

Each of these measurements is called a "tick", and it is the number of ticks, rather than the time, which is measured on the abscissa axis.

The pulse is made up of a fast-oscillating *carrier wave* $\sin\alpha t$ and a slowly varying *envelope* $P(\epsilon t)$, where $0 < \epsilon \ll 1$ is a small parameter to be defined later. Hence the received signal is given by

$$p_{\mathrm{R}}(t) = P(\epsilon t)\sin\beta t, \tag{3.1}$$

where the subscript "R" refers to "received". The quantity of interest is the envelope $A(\epsilon t)$, which is plotted on a log plot at the bottom of Fig. 3.1. But given data such as in the top of Fig. 3.1, how does one infer the envelope?

The answer lies in the *analytic signal*, which is related to the Hilbert transform. We give a *very* brief introduction for our purposes below; for more details, consult Bracewell

(2000). We recall the following transforms (Kammler, 2008):

$$\mathcal{F}\{P\sin\beta t\} = P\frac{\delta(\omega-\beta)-\delta(\omega+\beta)}{2i},$$
$$\mathcal{F}\left\{Pe^{i\beta t}\right\} = P\delta(\omega-\beta).$$

In other words, the $e^{i\beta t}$ has a single spike at $\omega=\beta$, while $\sin\beta t$ has two spikes at $\omega=\pm\beta$. In particular, we note from the above that

$$\mathcal{F}\left\{Pe^{i\beta t}\right\} = 2iH(\omega)\mathcal{F}\{P\sin\beta t\},$$

for constant P. Now (similar to a WKB analysis) we say that since $A(\epsilon t)$ varies on a slow scale, on the scale of the Fourier transform it behaves roughly like a constant (up to some $O(\epsilon)$ error). Hence we now say that

$$\begin{aligned}\mathcal{F}\left\{P(\epsilon t)e^{i\beta t}\right\} &\sim 2iH(\omega)\mathcal{F}\{P(\epsilon t)\sin\beta t\}\\ P(\epsilon t)e^{i\beta t} &\sim \mathcal{F}^{-1}\{2iH(\omega)\mathcal{F}\{p_{\mathrm{R}}(t)\}\}\\ P(\epsilon t) &\sim 2\left|\mathcal{F}^{-1}\{H(\omega)\hat{p}_{\mathrm{R}}(\omega)\}\right|.\end{aligned} \tag{3.2}$$

Equation (3.2) now shows how to construct the envelope. Take the Fourier transform of the received signal, remove the negative frequencies, and double the result. Then take the absolute value of the inverse Fourier transform of the result. (Note that in a real experimental setup, these will be finite Fourier transforms.)

To demonstrate the concept we introduce a modulated signal as the pulse and see what happens if we listen at a fixed distance from the transducer. Motivated by the problem statement, we use a truncated Gaussian for our envelope function:

$$p_{\mathrm{P}}(t) = \exp\left(-\frac{(t-\pi/\epsilon\omega)^2}{2\epsilon^2}\right)\left[H(t)-H\left(t-\frac{2\pi}{\epsilon\omega}\right)\right]\sin\omega t. \tag{3.3}$$

Some discussion of (3.3) is appropriate. In particular, we see that the signal lasts for $t\in[0,2\pi/\epsilon\omega]$. This then allows $O(\epsilon^{-1})$ carrier wave oscillations within the amplitude. The maximum of the envelope is centered on this range. This function is graphed in Fig. 3.2 for a value of ϵ that roughly replicates the form of the *received* wave in Fig. 3.1.

Now we substitute (3.3) into (2.17a) and graph the result for $\ell = 35c_{\mathrm{T}}/c_1$, which is shown as the solid line in Fig. 3.3. Here we have plotted the amount of time that corresponds to 20 echoes. To use the analytical signal, we sample points at every t_{s}, which we obtain from (2.18):

$$t_{\mathrm{s}} = \pi\frac{2f_{\mathrm{c}}}{f_{\mathrm{s}}} = \frac{2\pi}{8.25}\approx 0.76. \tag{3.4}$$

Once those points have been obtained, we perform the process described above to back out $A(t)$, which is shown as the dotted line in Fig. 3.3.

Note that the received signal in Fig. 3.3 has many more oscillations than the experimental data in Fig. 3.1. Hence modeling the transmitted signal by the received signal does not seem to be an appropriate strategy.

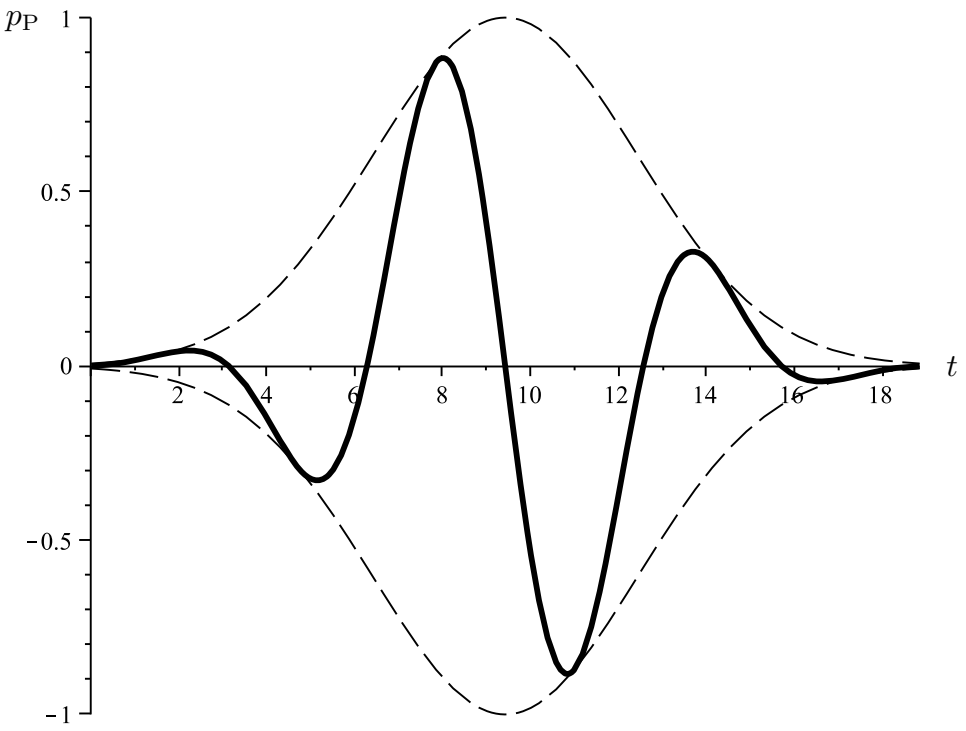

Figure 3.2. Input function $p_{\mathrm{P}}(t)$, $\omega = 1$, $\epsilon = 1/3$.

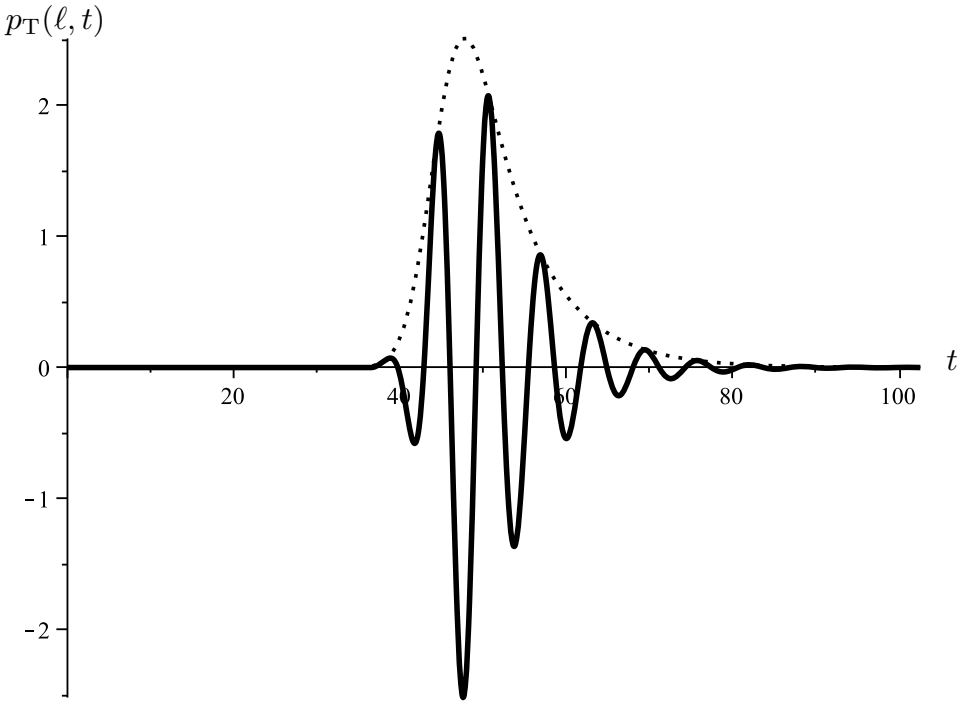

Figure 3.3. Received signal $p_{\mathrm{T}}(\ell, t)$, $\omega = 1$, $\epsilon = 1/3$, $R_{\mathrm{P}} = 1$, $R_{\mathrm{T}} = -0.63$, $\ell = 35/r$.

To match the data in Fig. 3.1, we take the base-10 logarithm of A and plot the result

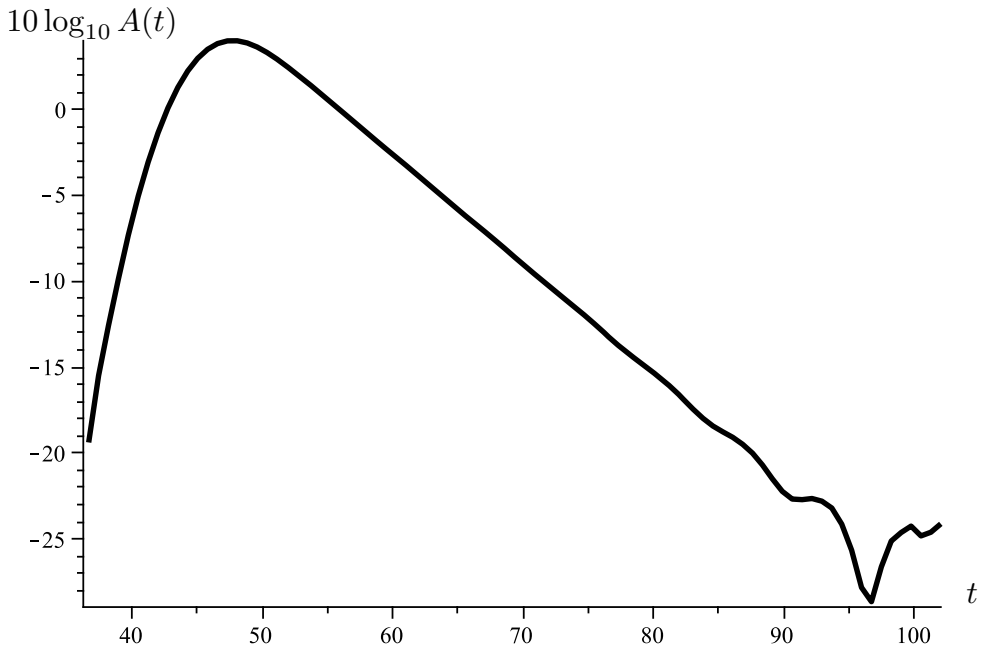

Figure 3.4. Decibel-scale plot of $A(t)$.

in Fig. 3.4. Note that there is some ringing for long time. Therefore, we have at least a "proof of concept" of ringing for the linear model.

But the position of the ringing is much different from that in the experimental data. Of course, we have not matched the experimental setup where the signal is measured back at $x = 0$ after bouncing off a reflector at $x = \ell$. In the next section we outline the mathematical analysis of such a system.

Section 4: Linear One-Layer Model, Incoming Wave

Next we briefly consider a model problem for the waves reflecting back from an object in the water. We use the same linear equations as in the previous section, which is more justifiable due to the small amplitude of the reflected waves. In this problem we send a pulse in from $x = \ell$ to the right, so

$$p(x, 0) = \delta(x - \ell). \tag{4.1}$$

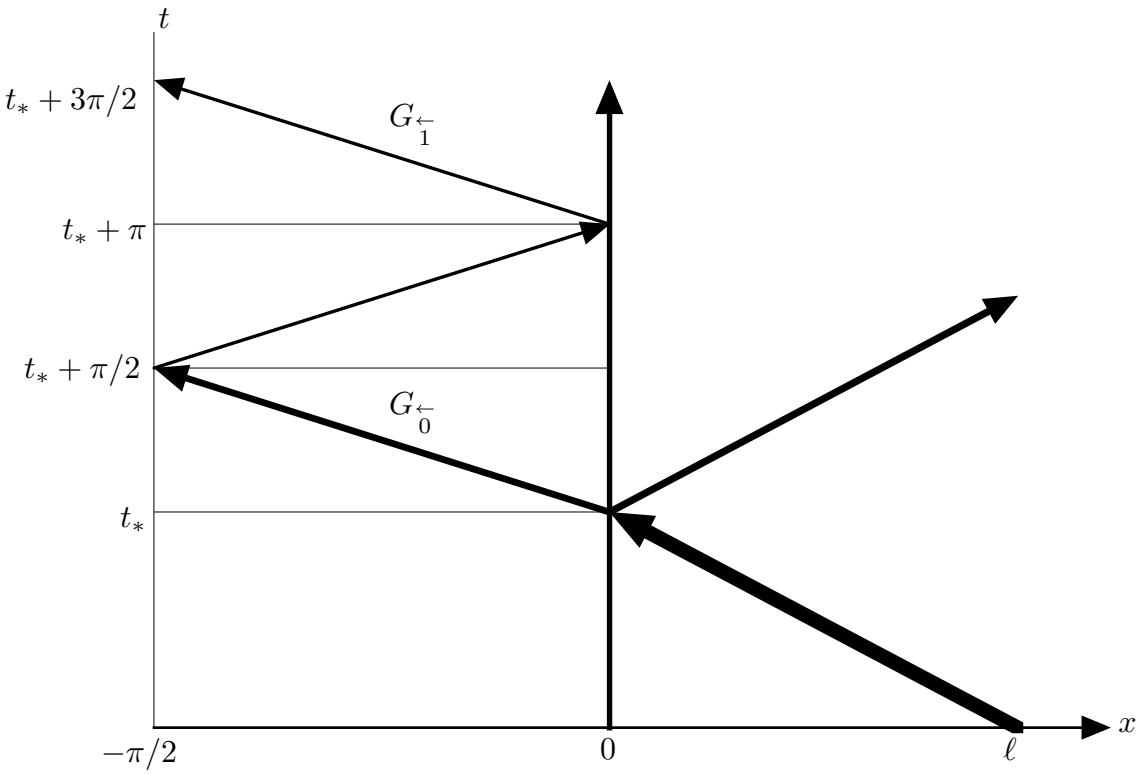

Figure 4.1. Characteristic diagram for Green's function, incoming wave.

The characteristic diagram is shown in Figure 4.1. Note the similarity to Figure 2.2. In particular, note that once the outcoming wave hits the layer at the to-be-determined time $t = t_*$, the problem is essentially exactly the same as that in section 2 with $t = \pi/2$ replaced by $t = t_*$ and a different amplitude to the wave. In particular, we have

$$G_{\mathrm{T}}(x, t) = \delta\left(x - \ell + \frac{t}{r}\right), \quad 0 < t < \ell r \equiv t_*. \tag{4.2}$$

When the wave hits the layer, part of the wave is reflected with reflection coefficient $-R_{\mathrm{T}}$, since the roles of Z_{T} and Z_1 are reversed. Note that this is positive, since the wave is

moving into a region of higher impedance. We assume that the water is semi-infinite, so this reflected wave is lost and does not play a role in the analysis. Hence the transmitted wave is the one of interest:

$$G_{\mathrm{L}}(x,t) = (1+R_{\mathrm{T}})\delta\left(x+(t-t_*)\right), \quad 0 < t-t_* < \frac{\pi}{2}, \tag{4.3}$$

where we again allow the interval of interest to move with x.

This transmitted wave then reflects again from the PZT boundary. We denote the reflection coefficient distinctly as R_{P}, though from the Appendix we see that the material is designed so $R_{\mathrm{P}} = -R_{\mathrm{T}}$. Hence we have

$$G_{\mathrm{L}}(x,t) = (1+R_{\mathrm{T}})R_{\mathrm{P}}\delta\left(x-(t-t_*)+\pi\right), \quad \pi/2 < t-t_* < \pi. \tag{4.4}$$

This wave will then reflect again, this time with reflection coefficient R_{T}, to yield

$$G_{\mathrm{L}}(x,t) = (1+R_{\mathrm{T}})R_{\mathrm{P}}R_{\mathrm{T}}\delta\left(x+(t-t_*)-\pi\right), \quad \pi < t-t_* < \frac{3\pi}{2}. \tag{4.5}$$

But this is just the expression for G_{L} in (4.3), scaled down by $R_{\mathrm{T}}R_{\mathrm{P}}$ and phase-shifted by π, and we have established our recursion pattern. We measure the signal at $x = -\pi/2$, so the true signal of interest is

$$G_{\mathrm{L}}\left(-\frac{\pi}{2},t\right) = \sum_{k=0}^{K} G_{\overset{\leftarrow}{k}}(t), \quad t-t_* \in \left[\frac{(2K+1)\pi}{2}, \frac{(2K+3)\pi}{2}\right], \tag{4.6a}$$

where $G_{\overset{\leftarrow}{k}}(t)$ is the kth echo measured at $x = -\pi/2$:

$$G_{\overset{\leftarrow}{k}}(t) = (1+R_{\mathrm{T}})(R_{\mathrm{P}}R_{\mathrm{T}})^k\delta\left(t-t_*-\frac{(2k+1)\pi}{2}\right). \tag{4.6b}$$

Note that $G_{\overset{\leftarrow}{k}}$ is a function of t only, since it is measured at a particular point ($x = -\pi/2$). The left-pointing arrow shows this is an echo of an incoming wave. Note the similarity in form between (4.6b) and (2.13). Again we have the attenuation factor $R_{\mathrm{P}}R_{\mathrm{T}}$ for each echo, and the travel time $k\pi$ (recalling that $r\ell = t_*$). The full result may be written in the form of an infinite series:

$$G_{\mathrm{L}}\left(-\frac{\pi}{2},t\right) = \sum_{k=0}^{\infty} G_{\overset{\leftarrow}{k}}(t). \tag{4.7a}$$

This result can then be used to construct analogous profiles to Fig. 3.3. In particular, for a general pressure function at $x = \ell$:

$$p_{\mathrm{T}}(\ell,t) = p_\ell(t),$$

the equation analogous to (2.17a) becomes

$$p_{\mathrm{L}}\left(-\frac{\pi}{2},t\right) = \sum_{k=0}^{K} p_{\overset{\leftarrow}{k}}(t), \quad t-t_* \in \left[\frac{(2K+1)\pi}{2}, \frac{(2K+3)\pi}{2}\right], \tag{4.8a}$$

$$p_{\overset{\leftarrow}{k}}(t) = (1+R_{\mathrm{T}})(R_{\mathrm{P}}R_{\mathrm{T}})^k p_\ell\left(t-t_*-\frac{(2k+1)\pi}{2}\right). \tag{4.8b}$$

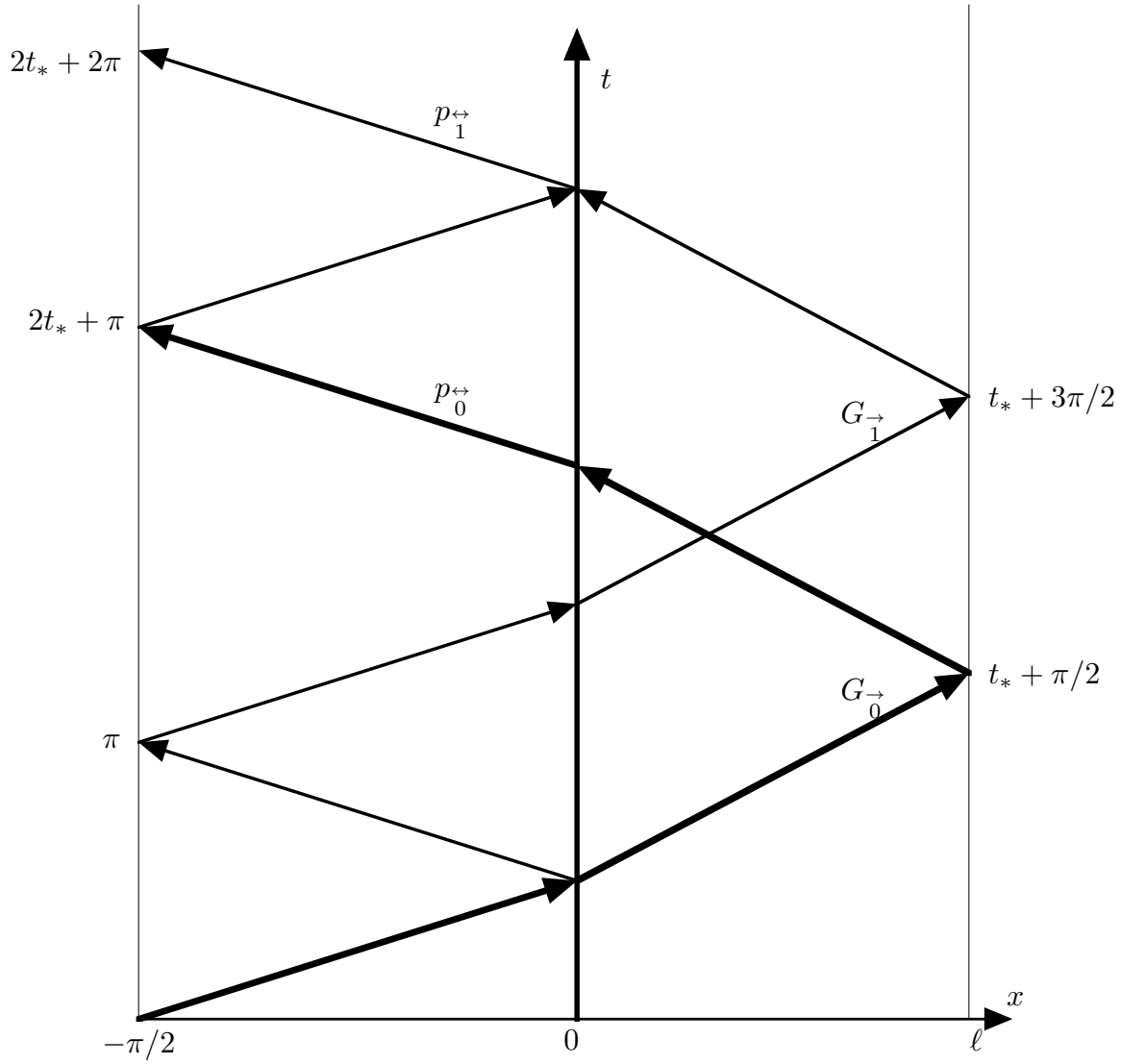

Figure 4.2. Characteristic diagram for Green's function, reflected wave.

Again K is the number of echoes that have had time to travel from $x = L$ back to $x = 0$, and k indexes them.

To try to follow an initial wave through a reflection, we first go back to the transmission of a single pulse in order to obtain insight. Substituting $x = \ell$ into (2.16), we have

$$G_{\mathrm{T}}(\ell, t) = \sum_{j=0}^{\infty} G_{\underset{j}{\rightarrow}}(\ell, t). \tag{4.9}$$

We assume perfect reflection at $x = \ell$, so $G_{\mathrm{T}}(\ell, t) = p_\ell(t)$. Hence we have

$$p_\ell\left(t - t_* - \frac{(2k+1)\pi}{2}\right) = \sum_{j=0}^{\infty} G_{\underset{j}{\rightarrow}}\left(\ell, t - t_* - \frac{(2k+1)\pi}{2}\right)$$

$$p_{\underset{k}{\leftarrow}}(t) = (1+R_{\mathrm{T}})(R_{\mathrm{P}}R_{\mathrm{T}})^k \times \sum_{j=0}^{\infty}(1-R_{\mathrm{T}})(R_{\mathrm{P}}R_{\mathrm{T}})^j \delta\left(\left(t - t_* - \frac{(2k+1)\pi}{2}\right) - j\pi - \frac{\pi}{2} - r\ell\right),$$

$$\begin{aligned} p_{\mathrm{L}}\left(-\frac{\pi}{2}, t\right) &= \sum_{k=0}^{\infty}(1+R_{\mathrm{T}})(R_{\mathrm{P}}R_{\mathrm{T}})^k \sum_{j=0}^{\infty}(1-R_{\mathrm{T}})(R_{\mathrm{P}}R_{\mathrm{T}})^j \delta(t - 2t_* - (j+k+1)\pi) \\ &= (1-R_{\mathrm{T}}^2)\sum_{k=0}^{\infty}\sum_{j=0}^{\infty}(R_{\mathrm{P}}R_{\mathrm{T}})^{j+k}\delta(t - 2t_* - (j+k+1)\pi), \end{aligned} \tag{4.10}$$

where we have used (2.13), (4.2), and (4.9). Note that the sum depends only on the combination $j+k$. This is shown in Fig. 4.2, where we see that the pulse that reflects once on the outgoing path ($j=1$, $k=0$) and the pulse that reflects once on the incoming path ($j=0$, $k=1$) recombine to form a single signal. Hence we may rewrite (4.10) as a single sum:

$$p_{\mathrm{L}}\left(-\frac{\pi}{2}, t\right) = (1-R_{\mathrm{T}}^2)\sum_{j=0}^{\infty}(R_{\mathrm{P}}R_{\mathrm{T}})^j \delta(t - 2t_* - (j+1)\pi). \tag{4.11}$$

Then for a general signal, we may derive an expression analogous to (2.17b):

$$p_{\mathrm{L}}\left(-\frac{\pi}{2}, t\right) = \sum_{j=0}^{J} p_{\underset{j}{\leftrightarrow}}(t), \qquad t - 2t_* \in [(J+1)\pi, (J+2)\pi], \tag{4.12a}$$

$$p_{\underset{j}{\leftrightarrow}}(t) = (1-R_{\mathrm{T}}^2)(R_{\mathrm{P}}R_{\mathrm{T}})^j p_{\mathrm{P}}(t - 2t_* - (j+1)\pi). \tag{4.12b}$$

Here the two-headed arrow has been used to show that this echo comes from reflection. Also, we assume that t_* is so long that the outgoing signal has been shut off before the reflections come back.

Section 5: Nonlinear Model

We now wish to incorporate nonlinear effects into our model. These effects occur if we treat the constitutive relation between density and pressure more carefully. In liquids, the Tate formula for the constitutive relation is (Naugolnykh, p. 4)

$$\tilde{p}(\tilde{\rho}) = \frac{c^2\rho_\mathrm{e}}{\gamma}\left(\frac{\tilde{\rho}}{\rho_\mathrm{e}}\right)^\gamma - \alpha, \tag{5.1}$$

where α and γ are constants and the subscript "e" refers to equilibrium state. Using the same notation for the pressure, we may rewrite (5.1) as

$$\begin{aligned}
\tilde{p} &= p_\mathrm{e} + \frac{c^2\rho_\mathrm{e}}{\gamma}\left[\left(\frac{\tilde{\rho}}{\rho_\mathrm{e}}\right)^\gamma - 1\right] \\
\left(\frac{\tilde{\rho}}{\rho_\mathrm{e}}\right)^\gamma &= 1 + \frac{\gamma(\tilde{p}-p_\mathrm{e})}{c^2\rho_\mathrm{e}} \\
\tilde{\rho} &= \rho_\mathrm{e}\left[1 + \frac{\gamma(\tilde{p}-p_\mathrm{e})}{c^2\rho_\mathrm{e}}\right]^{1/\gamma}.
\end{aligned} \tag{5.2}$$

From the values in the appendix, we know that while p_c may be much larger than p_e, it is not larger than $c^2\rho_\mathrm{e}$ (at least for water). Hence we introduce the following scalings:

$$\tilde{p} = p_\mathrm{e} + p_\mathrm{c}p = p_\mathrm{e} + \epsilon c^2\rho_\mathrm{e}p, \qquad \epsilon = \frac{p_\mathrm{c}}{c^2\rho_\mathrm{e}}. \tag{5.3}$$

Substituting (5.3) into (5.2), we obtain

$$\tilde{\rho} = \rho_\mathrm{e}\left(1 + \epsilon\gamma p\right)^{1/\gamma}, \tag{5.4}$$

which motivates the scaling

$$\tilde{\rho} = \rho_\mathrm{e}(1 + \epsilon\rho), \tag{5.5}$$

and hence we see that the density of the water doesn't vary much as a result of the pressure waves. Substituting (5.5) into (5.4) and expanding to leading two orders, we have

$$\begin{aligned}
\rho_\mathrm{e}(1+\epsilon\rho) &= \rho_\mathrm{e}\left[1 + \frac{\epsilon\gamma p}{\gamma} + \frac{(\epsilon\gamma p)^2}{2\gamma}\left(\frac{1}{\gamma} - 1\right)\right] \\
\rho &= p - \frac{\epsilon p^2(\gamma-1)}{2},
\end{aligned} \tag{5.6}$$

which, after some manipulation, is exactly (2.3) in Novikov, whose analysis we follow here.

But now we must careful, as the analysis is subtle. Suppose that we wanted to use an approximation for $y = e^z$ that included the first three terms:

$$y = e^z = 1 + z + \frac{z^2}{2}.$$

One way to justify this formally would be to set $y = 1 + \epsilon y_*$, $z = \epsilon z_*$, where $\epsilon \ll 1$, and expand

$$\begin{aligned} 1 + \epsilon y_* &= 1 + \epsilon z_* + \frac{(\epsilon z_*)^2}{2} \\ y_* &= z_* + \frac{\epsilon z_*^2}{2}. \end{aligned} \tag{5.7}$$

However, there is a problem with the above. If we continue to treat ϵ as a small parameter, then the quadratic term always appears at next order, which defeats the purpose of expanding as a quadratic in the first place. Therefore, to make sure that we keep both terms in (5.7), we must treat ϵ as an $O(1)$ parameter once we've done the expansion. To emphasize this, we add a subscript $*$ to the parameter and rewrite (5.7) as

$$y_* = z_* + \frac{\epsilon_* z_*^2}{2}.$$

Using this same sort of analysis in (5.6), we have

$$\rho = p - \frac{\epsilon_* p^2(\gamma - 1)}{2}. \tag{5.8}$$

We will eventually use our new scaled constitutive equation (5.8) in the Navier-Stokes equations. We begin with conservation of mass:

$$\begin{aligned} \frac{\partial \tilde{\rho}}{\partial \tilde{t}} + \frac{\partial(\tilde{\rho}\tilde{v})}{\partial \tilde{x}} &= 0 \\ \rho_{\mathrm{e}}\omega_{\mathrm{c}}\frac{\partial(1+\epsilon\rho)}{\partial t} + \rho_{\mathrm{e}}\frac{\omega_{\mathrm{c}}}{c_{\mathrm{T}}}\frac{\partial((1+\epsilon\rho)\tilde{v})}{\partial x} &= 0 \\ \epsilon\frac{\partial \rho}{\partial t} + \frac{1}{c_{\mathrm{T}}}\frac{\partial((1+\epsilon\rho)\tilde{v})}{\partial x} &= 0, \end{aligned} \tag{5.9}$$

where we have used (2.4) (translated to tissue) and (5.5). Equation (5.9) then motivates the following scaling for $\tilde{v}$:

$$v(x,t) = \frac{\tilde{v}(x,t)}{\epsilon c_{\mathrm{T}}}, \tag{5.10}$$

which implies that velocity displacements are small as well. Substituting (5.10), and (5.8) into (5.9), we obtain

$$\begin{aligned} \epsilon\frac{\partial}{\partial t}\left(p - \frac{\epsilon_* p^2(\gamma-1)}{2}\right) + \epsilon\frac{\partial}{\partial x}\left((1+\epsilon\rho)v\right) &= 0 \\ \frac{\partial p}{\partial t} + \frac{\partial v}{\partial x} - \epsilon_*\frac{(\gamma-1)}{2}\frac{\partial(p^2)}{\partial t} &= -\epsilon\frac{\partial(\rho v)}{\partial x}, \end{aligned} \tag{5.11}$$

where we have retained terms only up to $O(\epsilon)$.

The dimensionless form of the momentum equation is derived as follows:

$$\begin{aligned}
\tilde{\rho}\left(\frac{\partial \tilde{v}}{\partial \tilde{t}}+\tilde{v}\frac{\partial \tilde{v}}{\partial \tilde{x}}\right) &= -\frac{\partial \tilde{p}}{\partial \tilde{x}}+\mu\frac{\partial^2 \tilde{v}}{\partial \tilde{x}^2} \\
\rho_{\mathrm{e}}(1+\epsilon\rho)\left[\epsilon c_{\mathrm{T}}\omega_{\mathrm{c}}\frac{\partial v}{\partial t}+(\epsilon c_{\mathrm{T}})^2\frac{\omega_{\mathrm{c}}}{c_{\mathrm{T}}}v\frac{\partial v}{\partial x}\right] &= -\frac{\omega_{\mathrm{c}}}{c_{\mathrm{T}}}\frac{\partial(p_{\mathrm{e}}+\epsilon c_{\mathrm{T}}^2\rho_{\mathrm{e}}p)}{\partial x}+\mu\epsilon c_{\mathrm{T}}\left(\frac{\omega_{\mathrm{c}}}{c_{\mathrm{T}}}\right)^2\frac{\partial^2 v}{\partial x^2} \\
(1+\epsilon\rho)\left(\frac{\partial v}{\partial t}+\epsilon v\frac{\partial v}{\partial x}\right) &= -\frac{\partial p}{\partial x}+\frac{\mu\omega_{\mathrm{c}}}{\rho_{\mathrm{e}}c_{\mathrm{T}}^2}\frac{\partial^2 v}{\partial x^2} \\
\frac{\partial v}{\partial t}+\frac{\partial p}{\partial x}-\eta\frac{\partial^2 v}{\partial x^2} &= -\epsilon\left(\rho\frac{\partial v}{\partial t}+v\frac{\partial v}{\partial x}\right), \quad \eta=\frac{\mu\omega_{\mathrm{c}}}{\rho_{\mathrm{e}}c_{\mathrm{T}}^2}.
\end{aligned} \tag{5.12}$$

where μ is the bulk viscosity, and we have again only kept terms to $O(\epsilon)$.

From the values in the Appendix, we see that η is very small, which says that viscous dissipation is very small in water. This is consistent with our intuition about underwater acoustics. In Girynk *et al.*, the authors calculate a value for μ in soft tissue that is several orders of magnitude higher, which drives η close to $O(1)$.

Taking the t derivative of (5.11) and subtracting the x derivative of (5.12), we obtain

$$\frac{\partial^2 p}{\partial t^2}-\epsilon_*\frac{(\gamma-1)}{2}\frac{\partial^2(p^2)}{\partial t^2}-\frac{\partial^2 p}{\partial x^2}+\eta\frac{\partial^2 v}{\partial x^3}=-\epsilon\frac{\partial^2(\rho v)}{\partial x\partial t}+\epsilon\frac{\partial}{\partial x}\left(\rho\frac{\partial v}{\partial t}+v\frac{\partial v}{\partial x}\right). \tag{5.13}$$

Now we wish to write our leading-order equation in terms of p alone. There are many tricks to do this, depending on the book used. For our purposes, we use the fact that η is somewhat small to *temporarily* write $\eta=\eta_*\epsilon^{1/2}$, and then keep all terms "at leading order" (on the left-hand side) which are $O(\epsilon^{1/2})$ or greater.

To write the viscous term in terms of the pressure, we take the second derivative of (5.11) with respect to x and substitute the result into (5.13), yielding

$$\begin{aligned}
\frac{\partial^2 p}{\partial t^2}-\epsilon_*\frac{(\gamma-1)}{2}\frac{\partial^2(p^2)}{\partial t^2}-\frac{\partial^2 p}{\partial x^2}-\eta_*\epsilon^{1/2}\frac{\partial^3 p}{\partial x^2\partial t}+\epsilon_*\eta_*\epsilon^{1/2}\frac{(\gamma-1)}{2}\frac{\partial^3(p^2)}{\partial x^2\partial t} \\
=\epsilon\frac{\partial}{\partial x}\left(v\left(\frac{\partial v}{\partial x}-\frac{\partial \rho}{\partial t}\right)\right)+\eta_*\epsilon^{3/2}\frac{\partial^3(\rho v)}{\partial x^3}.
\end{aligned} \tag{5.14}$$

But now consider the last term on the first line. It now behaves like $\epsilon^{3/2}$, which is smaller than the terms we decided to keep when using the quadratic expansion. Hence it is moved over to the right-hand side as well:

$$\begin{aligned}
\frac{\partial^2 p}{\partial t^2}-\epsilon_*\frac{(\gamma-1)}{2}\frac{\partial^2(p^2)}{\partial t^2}-\frac{\partial^2 p}{\partial x^2}-\eta_*\epsilon^{1/2}\frac{\partial^3 p}{\partial x^2\partial t} \\
=\epsilon\frac{\partial}{\partial x}\left(v\left(\frac{\partial v}{\partial x}-\frac{\partial \rho}{\partial t}\right)\right)+\eta_*\epsilon^{3/2}\left[\frac{\partial^3(\rho v)}{\partial x^3}-\frac{(\gamma-1)}{2}\frac{\partial^3(p^2)}{\partial x^2\partial t}\right].
\end{aligned} \tag{5.15}$$

Therefore, we may write the leading-order form as

$$\frac{\partial^2 p}{\partial t^2}-\epsilon_*\frac{(\gamma-1)}{2}\frac{\partial^2(p^2)}{\partial t^2}-\frac{\partial^2 p}{\partial x^2}-\eta\frac{\partial^3 p}{\partial x^2\partial t}=0, \tag{5.16}$$

as in Novikov. Other books use the *Westervelt approximation*, as follows. Working with the top line of (5.14), we have

$$\begin{aligned}\frac{\partial^2 p}{\partial x^2} &= \frac{\partial^2 p}{\partial t^2} - \epsilon_* \frac{(\gamma-1)}{2}\frac{\partial^2 (p^2)}{\partial t^2} + \eta_* \epsilon^{1/2} \frac{\partial^2 p}{\partial x^2 \partial t} + o(\epsilon^{1/2}) \\ \eta_* \epsilon^{1/2} \frac{\partial^2 p}{\partial x^2} &= \eta_* \epsilon^{1/2} \frac{\partial^2 p}{\partial t^2} + o(\epsilon^{1/2}),\end{aligned} \tag{5.17}$$

where we have again used the trick where $\epsilon_* \epsilon^{1/2}$ is taken to be small. Substituting this into the top line of (5.14), the x-derivatives on p get swapped for t-derivatives and we have

$$\frac{\partial^2 p}{\partial t^2} - \epsilon_* \frac{(\gamma-1)}{2}\frac{\partial^2 (p^2)}{\partial t^2} - \frac{\partial^2 p}{\partial x^2} - \eta \frac{\partial^3 p}{\partial t^3} = 0, \tag{5.18}$$

as in Hamilton. However, since we are moving to the traveling wave coordinate system soon, this is a distinction without a difference.

Section 6: Envelope Equations

The Westervelt approximation yields a nonlinear partial differential equation that is second-order in space and third-order in time. For our purposes, it is a singularly perturbed two-way wave equation with signalling data issued at the leftmost boundary that consists of a slowly modulated pulse-like envelope containing a rapidly varying carrier frequency. It is convenient to exploit this disparity in scales in order to obtain envelope equations that are analytically and computationally more tractable.

We start from a form of (5.18) that includes an additional term to account for bulk scattering,

$$\frac{\partial^2 p}{\partial t^2} - \frac{\epsilon_*(\gamma-1)}{2}\frac{\partial^2 (p^2)}{\partial t^2} - \frac{\partial^2 p}{\partial x^2} - \eta\frac{\partial^3 p}{\partial t^3} + \beta\frac{\partial p}{\partial t} = 0. \tag{6.1}$$

Noting that the carrier frequency has already been normalized in the above equation, we introduce the small parameter $\delta = 2\pi/T_{\mathrm{P}}$, where T_{P} is a characteristic (dimensionless) temporal pulse width produced at the transducer. We argue on physical grounds that nonlinearity, viscosity and scattering are all small and of the same order for a dominant balance. For reasons that will become clear later, we choose them all to be $O(\delta^{-2})$, leading us to write their coefficients in the following form:

$$\frac{\epsilon_*(\gamma-1)}{2} \equiv \delta^2\epsilon_2, \qquad \eta \equiv \delta^2\eta_2, \quad \text{and} \quad \beta \equiv \delta^2\beta_2. \tag{6.2}$$

Thus, we arrive at the rescaled equation

$$\frac{\partial^2 p}{\partial t^2} - \frac{\partial^2 p}{\partial x^2} = \delta^2\left[\epsilon_2\frac{\partial^2 (p^2)}{\partial t^2} + \eta_2\frac{\partial^3 p}{\partial t^3} - \beta_2\frac{\partial p}{\partial t}\right]. \tag{6.3}$$

where we assume that the data have amplitude of order unity.

In keeping with the slowly varying envelope approximation (SVEA), we introduce multiple time and spatial scales, $x_n = \delta^n x$ and $t_n = \delta^n t$, and a solution in the form of asymptotic series whose terms depend on all variables, i.e.,

$$p(x,t) = p_0(x_0, t_0, x_1, t_1, \ldots) + \delta p_1(x_0, t_0, \ldots) + O(\delta^2). \tag{6.4}$$

We insert this Ansätz into (6.3), at each order setting inhomogeneous terms to zero that would lead to secular growth in the asymptotic series above.

At first order, we simply have the homogeneous wave equation,

$$\left(\frac{\partial^2}{\partial t_0^2} - \frac{\partial^2}{\partial x_0^2}\right) p_0 = 0, \tag{6.5}$$

which has the standard d'Alembert solution of left- and right-moving waves. We work in the complex plane and take a single mode of the right-moving solution

$$p_0 = P_0(x_1, t_1, \ldots)e^{i\theta_0} + \bar{P}_0 e^{-i\theta_0}, \tag{6.6}$$

where $\theta_j = x_j - t_j$. Due to the nonlinearity in the equation, we cannot simply take the real or imaginary part of the complex solution. However, using complex variables does simplify later algebra. In the rest of this section, we will write the complex conjugate terms as "c.c.", and not treat them separately unless necessary.

Note also that the form in (6.6) reflects the underlying assumption of a slowly modulated enveloped modifying a rapidly varying carrier oscillation.

At $O(\delta)$, we have

$$\begin{aligned}\left(\frac{\partial^2}{\partial t_0^2} - \frac{\partial^2}{\partial x_0^2}\right) p_1 &= -2\left(\frac{\partial^2 p_0}{\partial t_1 \partial t_0} - \frac{\partial^2 p_0}{\partial x_1 \partial x_0}\right) \\ &= 2i\left(\frac{\partial P_0}{\partial t_1} + \frac{\partial P_0}{\partial x_1}\right) e^{i\theta_0} + \text{c.c.} \end{aligned} \tag{6.7}$$

But we note that for any constant τ,

$$\left(\frac{\partial^2}{\partial t_0^2} - \frac{\partial^2}{\partial x_0^2}\right) p_1 = e^{i\tau\theta_0} \qquad \Longrightarrow \qquad p_1 = \frac{x_0}{i\tau} e^{i\tau\theta_0} + \cdots,$$

which is unbounded. Hence we must suppress the secular term on the right-hand side of (6.7), which yields

$$\frac{\partial P_0}{\partial x_1} = -\frac{\partial P_0}{\partial t_1} \tag{6.8a}$$

$$P_0 = P_0(\theta_1, x_2, t_2, \ldots). \tag{6.8b}$$

At this point, we simply observe that p_1 will also satisfy the homogeneous wave equation in x_0 and t_0; its particular functional form will be dictated by the next order, however.

At $O(\delta^2)$, we have, after substituting in the appropriate form of p_0,

$$\begin{aligned}&\left(\frac{\partial^2}{\partial t_0^2} - \frac{\partial^2}{\partial x_0^2}\right) p_2 + 2\left(\frac{\partial^2}{\partial t_0 \partial t_1} - \frac{\partial^2}{\partial x_0 \partial x_1}\right) p_1 + \left(\frac{\partial^2}{\partial t_1^2} - \frac{\partial^2}{\partial x_1^2}\right) p_0 \\ &\qquad + 2\left(\frac{\partial^2}{\partial t_0 \partial t_2} - \frac{\partial^2}{\partial x_0 \partial x_2}\right) p_0 = \epsilon_2 \frac{\partial^2 (p_0^2)}{\partial t_0^2} + \eta_2 \frac{\partial^3 p_0}{\partial t_0^3} - \beta_2 \frac{\partial p_0}{\partial t_0} \\ &\left(\frac{\partial^2}{\partial t_0^2} - \frac{\partial^2}{\partial x_0^2}\right) p_2 = -2\frac{\partial^2 p_1}{\partial t_0 \partial t_1} + 2\frac{\partial^2 p_1}{\partial x_0 \partial x_1} + 2i\left(\frac{\partial}{\partial t_2} + \frac{\partial}{\partial x_2}\right) P_0 e^{i\theta_0} \\ &\qquad - 4\epsilon_2 P_0^2 e^{2i\theta_0} + i(\eta_2 + \beta_2) P_0 e^{i\theta_0} + \text{c.c.} \end{aligned} \tag{6.9}$$

Since the cross-terms in p_0^2 due to the complex conjugate are constant, they do not survive the differentiation with respect to t_0.

The next step is to suppress the secularity. Since we are using an infinite set of slow variables, we have the necessary flexibility to suppress the $e^{i\theta}$ secularity by using only P_0:

$$\left(\frac{\partial}{\partial t_2} + \frac{\partial}{\partial x_2}\right) P_0 = -\frac{1}{2}(\eta_2 + \beta_2) P_0, \tag{6.10}$$

However, to suppress the $e^{2i\theta}$ secularity, we must introduce a functional form of p_1 that includes the second harmonic:

$$p_1 = P_1(x_1, t_1, x_2, t_2, \ldots)e^{2i\theta} + \text{c.c.}, \tag{6.11}$$

which yields

$$\left(\frac{\partial}{\partial t_1} + \frac{\partial}{\partial x_1}\right) P_1 = -i\epsilon_2 P_0^2. \tag{6.12}$$

We follow this method throughout, suppressing existing harmonics using existing terms in the analysis, while introducing new lower-order terms only for new harmonics. Hence as before, we leave p_2 unspecified for now to allow for suppression of secular terms at the next order.

Finally, at $O(\delta^3)$ we see how the second harmonic couples back to the fundamental wave, as we have

$$\begin{aligned}
&\left(\frac{\partial^2}{\partial t_0^2} - \frac{\partial^2}{\partial x_0^2}\right) p_3 + 2\left(\frac{\partial^2}{\partial t_0 \partial t_1} - \frac{\partial^2}{\partial x_0 \partial x_1}\right) p_2 + \left(\frac{\partial^2}{\partial t_1^2} - \frac{\partial^2}{\partial x_1^2}\right) p_1 \\
&\quad + 2\left(\frac{\partial^2}{\partial t_0 \partial t_2} - \frac{\partial^2}{\partial x_0 \partial x_2}\right) p_1 + 2\left(\frac{\partial^2}{\partial t_0 \partial t_3} - \frac{\partial^2}{\partial x_0 \partial x_3}\right) p_0 + 2\left(\frac{\partial^2}{\partial t_1 \partial t_2} - \frac{\partial^2}{\partial x_1 \partial x_2}\right) p_0 \\
&\qquad = 2\epsilon_2 \frac{\partial^2 (p_0^2)}{\partial t_0 \partial t_1} + 2\epsilon_2 \frac{\partial^2 (p_0 p_1)}{\partial t_0^2} + \eta_2 \frac{\partial^3 p_1}{\partial t_0^3} + 3\eta_2 \frac{\partial^3 p_0}{\partial t_0^2 \partial t_1} - \beta_2 \frac{\partial p_1}{\partial t_0} - \beta_2 \frac{\partial p_0}{\partial t_1} \\
&\left(\frac{\partial^2}{\partial t_0^2} - \frac{\partial^2}{\partial x_0^2}\right) p_3 + 2\left(\frac{\partial^2}{\partial t_0 \partial t_1} - \frac{\partial^2}{\partial x_0 \partial x_1}\right) p_2 + \left(\frac{\partial^2}{\partial t_1^2} - \frac{\partial^2}{\partial x_1^2}\right) P_1 e^{2i\theta_0} \\
&\quad - 4i\left(\frac{\partial}{\partial t_2} + \frac{\partial}{\partial x_2}\right) P_1 e^{2i\theta_0} - 2i\left(\frac{\partial}{\partial t_3} + \frac{\partial}{\partial x_3}\right) P_0 e^{i\theta_0} + 2\left(\frac{\partial}{\partial t_2} + \frac{\partial}{\partial x_2}\right) \frac{\partial P_0}{\partial t_1} e^{i\theta_0} \\
&\qquad = -4i\epsilon_2 \frac{\partial (P_0^2)}{\partial t_1} e^{2i\theta_0} + 2\epsilon_2 \frac{\partial^2 (P_0 P_1 e^{3i\theta} + \bar{P}_0 P_1 e^{i\theta})}{\partial t_0^2} + 8i\eta_2 P_1 e^{2i\theta_0} - 3\eta_2 \frac{\partial P_0}{\partial t_1} e^{i\theta_0} \\
&\qquad\qquad + 2i\beta_2 P_1 e^{2i\theta_0} - \beta_2 \frac{\partial P_0}{\partial t_1} e^{i\theta_0} + \text{c.c}, \qquad (6.13)
\end{aligned}$$

where we have used (6.6), (6.8a), and (6.11). (Again the cross-term in P_0^2 does not survive.) Hence there is now a third harmonic to be suppressed, requiring the following functional form for p_2:

$$p_2 = P_2(x_1, t_1, \cdots)e^{3i\theta_0} + \text{c.c.} \tag{6.14}$$

Substituting (6.14) into (6.13) and grouping by mode, we have

$$\begin{aligned}
&\left(\frac{\partial^2}{\partial t_0^2} - \frac{\partial^2}{\partial x_0^2}\right) p_3 = \left[6i\left(\frac{\partial}{\partial t_1} + \frac{\partial}{\partial x_1}\right) P_2 - 18\epsilon_2 P_0 P_1\right] e^{3i\theta} \\
&\quad + \left[-\left(\frac{\partial}{\partial t_1} - \frac{\partial}{\partial x_1}\right)(-i\epsilon_2 P_0^2) + 4i\left(\frac{\partial}{\partial t_2} + \frac{\partial}{\partial x_2}\right) P_1 + 8i\eta_2 P_1 + 2i\beta_2 P_1\right. \\
&\qquad \left. -4i\epsilon_2 \frac{\partial (P_0^2)}{\partial t_1}\right] e^{2i\theta_0} + \left[2i\left(\frac{\partial}{\partial t_3} + \frac{\partial}{\partial x_3}\right) P_0 + (\eta_2 + \beta_2)\frac{\partial P_0}{\partial t_1} - 2\epsilon_2 \bar{P}_0 P_1\right. \\
&\qquad\qquad \left. -(3\eta_2 + \beta_2)\frac{\partial P_0}{\partial t_1}\right] e^{i\theta_0} + \text{c.c.}, \qquad (6.15)
\end{aligned}$$

where we have used (6.10) and (6.12). Then suppressing each mode, we have

$$\left(\frac{\partial}{\partial t_1}+\frac{\partial}{\partial x_1}\right)P_2=-3i\epsilon_2P_0P_1, \tag{6.16a}$$

$$4i\left(\frac{\partial}{\partial t_2}+\frac{\partial}{\partial x_2}\right)P_1=-2i\epsilon_2\frac{\partial(P_0^2)}{\partial t_1}-2i(4\eta_2+\beta_2)P_1+4i\epsilon_2\frac{\partial(P_0^2)}{\partial t_1}$$

$$\left(\frac{\partial}{\partial t_2}+\frac{\partial}{\partial x_2}\right)P_1=-\left(2\eta_2+\frac{1}{2}\beta_2\right)P_1+\epsilon_2P_0\frac{\partial P_0}{\partial t_1}, \tag{6.16b}$$

$$\left(\frac{\partial}{\partial t_3}+\frac{\partial}{\partial x_3}\right)P_0=-i\eta_2\frac{\partial P_0}{\partial t_1}-i\epsilon_2\bar{P}_0P_1, \tag{6.16c}$$

where we have used (6.12). Equations (6.16) are called the *envelope equations*.

If we now multiply (6.8a), (6.10), and (6.16c) by the appropriate power of δ and sum, we obtain an expression for the derivative with respect to the unexpanded variables:

$$\sum_{j=1}^{3}\delta^j\left(\frac{\partial}{\partial t_j}+\frac{\partial}{\partial x_j}\right)P_0=-\frac{1}{2}\delta^2(\eta_2+\beta_2)P_0-i\delta^3\eta_2\frac{\partial P_0}{\partial t_1}-i\delta^3\epsilon_2\bar{P}_0P_1$$

$$\left(\frac{\partial}{\partial t}+\frac{\partial}{\partial x}\right)P_0=-\frac{1}{2}\delta^2(\eta_2+\beta_2)P_0-i\delta^2\eta_2\frac{\partial P_0}{\partial t}-i\delta^3\epsilon_2\bar{P}_0P_1+O(\delta^4), \tag{6.17a}$$

where we have used the fact that P_0 is independent of t_0. Also note that the second term on the right-hand side is formally of $O(\delta^3)$, since P_0 varies slowly with t. We may perform a similar analysis for P_1 using (6.12) and (6.16b) and P_2 to obtain

$$\sum_{j=1}^{2}\delta^j\left(\frac{\partial}{\partial t_j}+\frac{\partial}{\partial x_j}\right)P_1=-i\delta\epsilon_2P_0^2-\delta^2\left(2\eta_2+\frac{1}{2}\beta_2\right)P_1+\delta^2\epsilon_2P_0\frac{\partial P_0}{\partial t_1}$$

$$\left(\frac{\partial}{\partial t}+\frac{\partial}{\partial x}\right)P_1=-i\delta\epsilon_2P_0^2-\delta^2\left(2\eta_2+\frac{1}{2}\beta_2\right)P_1+\delta\epsilon_2P_0\frac{\partial P_0}{\partial t}+O(\delta^3), \tag{6.17b}$$

where again the third term on the right-hand side is formally of $O(\delta^2)$. Lastly, using (6.16a), we obtain the analogous equation for P_2:

$$\delta\left(\frac{\partial}{\partial t_1}+\frac{\partial}{\partial x_1}\right)P_2=-3i\delta\epsilon_2P_0P_1$$

$$\left(\frac{\partial}{\partial t}+\frac{\partial}{\partial x}\right)P_2=-3i\delta\epsilon_2P_0P_1+O(\delta^2). \tag{6.17c}$$

Then using our harmonics, we have that the full pressure field $p(x,t)$ is given asymptotically by

$$p(x,t)=P_0(x,t)e^{i(x-t)}+\delta P_1(x,t)e^{2i(x-t)}+\delta^2P_2(x,t)e^{3i(x-t)}+\text{c.c.}+O(\delta^3).$$

(Note that the error in p due to our computed solutions will be $O(\delta^4)$.) Equations (6.17) are the *envelope equations* for the Westervelt approximation. We observe the following features from their form:

- They are essentially one-way wave equations, greatly simplifying either analysis or computation.
- Each successive order in δ introduces coupling to the next harmonic. At the order given above, the third harmonic is driven by the lower harmonics; however, the first two harmonics form a closed system.
- The two damping mechanisms, viscous diffusion and bulk scattering, have an identical impact on the leading order, but have different effects on successive orders. This is due to the fact that successive orders represent higher harmonics, and diffusion affects these higher frequencies more severely.

Finally, we observe that while (6.17a) and (6.17b) have no obvious closed-form solution, if we stop at one order earlier, we obtain the system

$$\left(\frac{\partial}{\partial t}+\frac{\partial}{\partial x}\right)P_0 = -\frac{1}{2}\delta^2(\eta_2+\beta_2)P_0, \tag{6.18a}$$

$$\left(\frac{\partial}{\partial t}+\frac{\partial}{\partial x}\right)P_1 = -i\delta\epsilon_2 P_0^2, \tag{6.18b}$$

where we have used the fact that the derivative terms on the right-hand side of (6.17a) and (6.17b) are really one order smaller than they are displayed. Equations (6.18) can be solved subject to signalling data

$$P_0(0,t) = f(t), \quad P_1(0,t) = 0$$

to give

$$P_0(x,t) = f(t-x)\exp(-\frac{1}{2}\delta^2(\eta_2+\beta_2)x) \tag{6.19a}$$

$$P_1(x,t) = -\frac{i\epsilon_2 f^2(t-x)}{\delta(\eta_2+\beta_2)}\left(1-e^{-\delta^2(\eta_2+\beta_2)x}\right). \tag{6.19b}$$

The form of (6.19b) would seem to violate our perturbation assumption where each term should be smaller than the last. However, for $x = O(\delta^{-1})$, we see that $P_1 = O(1)$, as required.

Figure 6.1 depicts a signal formed by a single pulse and five subsequent shifted superposed copies of the original pulse with geometrically decreasing amplitudes. The signal is propagated through the medium using (6.19a) and (6.19b).

Figure 6.2 shows the growth in the second harmonic, which can be thought of as either draining energy from the fundamental mode or as distorting the primary pulse, where the nonlinear effects are strongest. Both phenomena decrease and possibly destroy the effectiveness of the linear-based filter method.

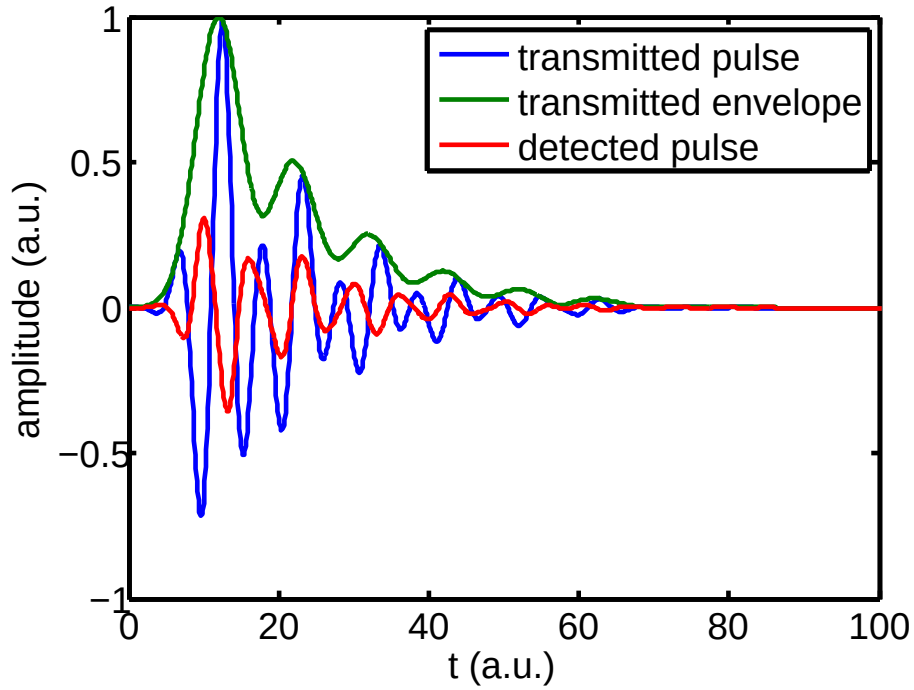

Figure 6.1. Transmitted signal composed of original pulse and five shifted, attenuated superposed copies, and received signal resulting from propagation through dissipative nonlinear medium.

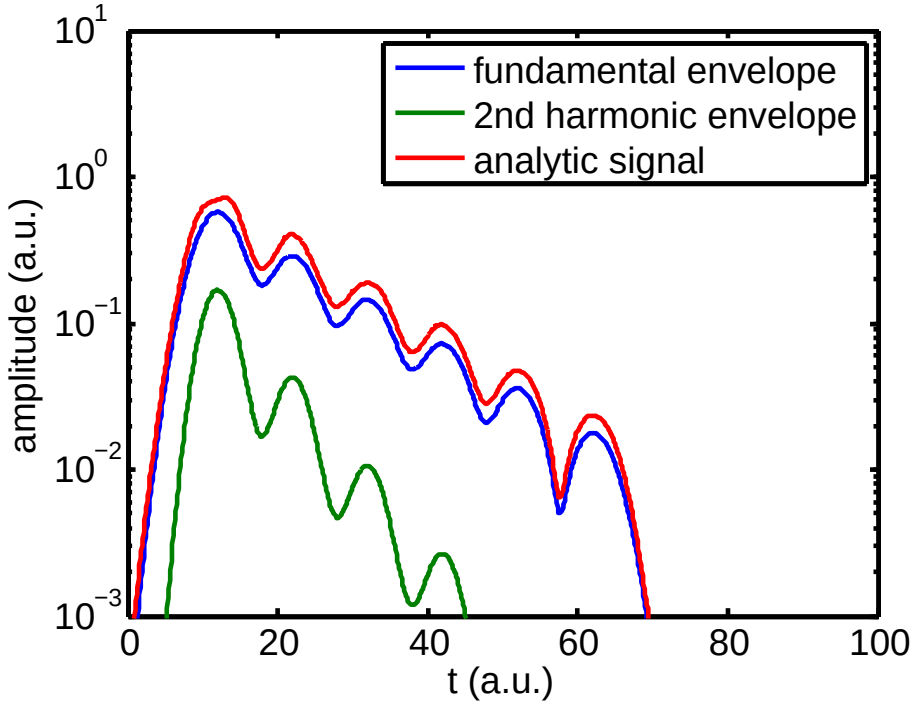

Figure 6.2. Numerically obtained envelopes of the fundamental and 2^{nd} harmonic frequencies after propagation through the medium.

Section 7: Signal Processing Ideas

The ringing effects in Fig. 4.1 obscure the true nature of the reflected signal. Hence it is advantageous to remove them. Currently they are removed through signal processing software as follows.

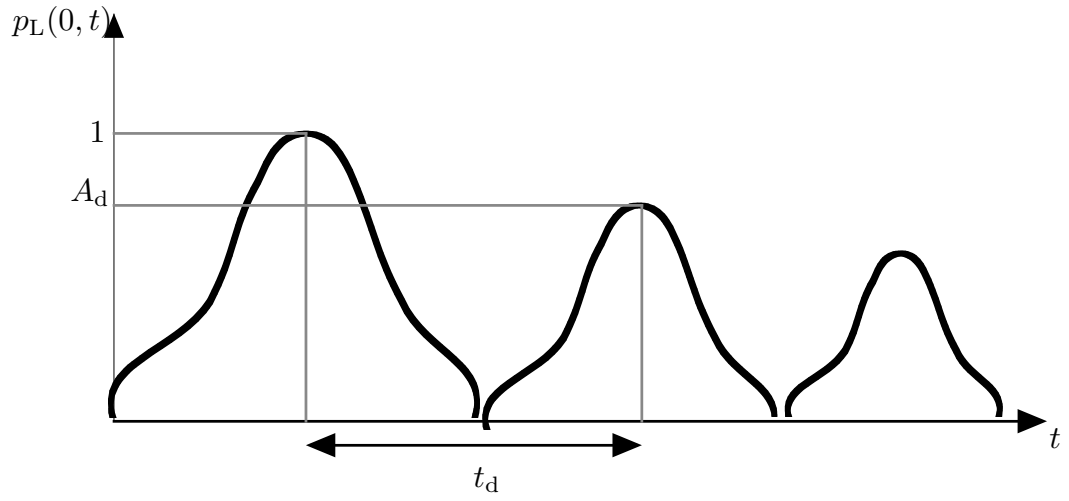

Figure 7.1. Schematic of received signal.

Consider an idealized experiment where the received signal consists of a series of discrete copies (not described as echoes, for reasons described below) of the first received pulse, each phase-shifted and scaled down. At first glance, this may seem inconsistent with the superposition shown in Fig. 2.3, but recall that that diagram refers to the initial signal *emitted*, while this model assumes copies of the first signal *received*.

Since the copies are assumed exact, one can remove the second lobe entirely by computing the ratio A_{d} (where the subscript "d" stands for "delay") of the amplitudes of the first and second humps, and t_{d} the distance between them. Then the postprocessed signal

$$p_{\mathrm{L}}(0,t) - A_{\mathrm{d}} p_{\mathrm{L}}(0, t - t_{\mathrm{d}})$$

will have the second hump removed, but the third hump will only be smaller, as shown in Fig. 7.2.

Then this process can be repeated as often as necessary to remove successive humps and refine the signal. Unfortunately, the computation of the A_{d} are too expensive to do in real-time, and so the parameters from the experimental setup in the water tank must be hard-coded into the software. But the signals reflected in tissue can be quite different.

Moreover, in the laboratory they run two experiments: one with low power in the linear regime and one with higher power in the nonlinear regime. Using this approach with the nonlinear data does not work as well. This was the original problem that was brought to the workshop.

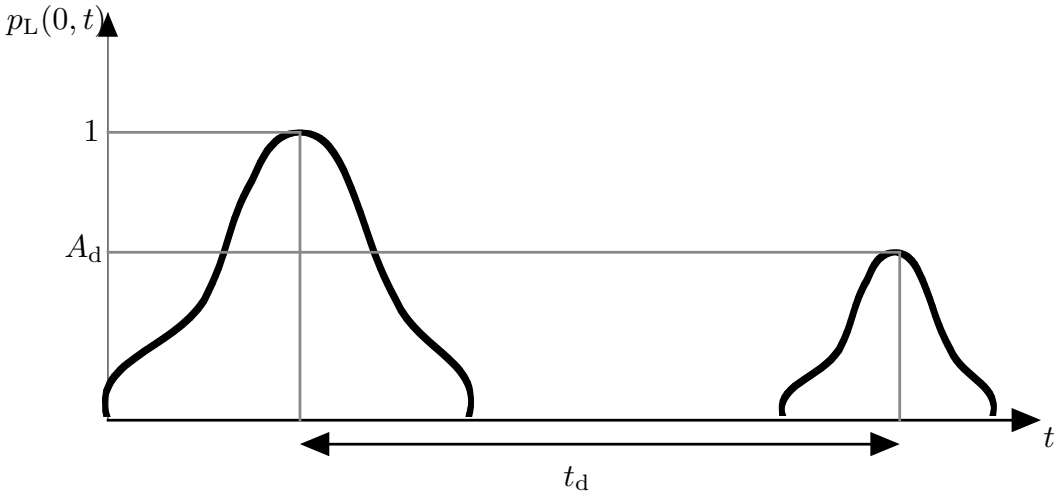

Figure 7.2. Schematic of received signal.

Hence a group at the workshop worked on the *empirical mode decomposition* (EMD) signal processing method.

Empirical Mode Decomposition

The Empirical Mode Decomposition (EMD) is a novel signal processing method introduced by Huang, et al. (1998). The EMD method is an empirically-based method. It is a spectral analysis method meant for signals coming from underlying processes that are nonlinear and non-stationary (aperiodic) in nature. The purpose of the method is to empirically extract components of the signal corresponding to separate time scales inherent in the signal. This is done through a process known as sifting. The extracted signals (called intrinsic mode functions, or IMFs) give a full decomposition of the signal in the sense that taking their sum returns the original signal. The intrinsic mode functions are different from the familiar Fourier modes because their frequency can vary locally and because they need not be periodic. Each of the individual IMFs can then be studied and can typically be linked to the separate physical phenomena that are present in the problem. For our problem, the reasoning behind using this method was the hope that performing the EMD on the data would isolate the desired part of the ultrasound signal and the ringdown artifacts into separate IMFs, thus separating the desired part of the signal and removing the unwanted artifacts.

Sifting process

An intrinsic mode function is a set of data satisfying two properties: (1) in the whole data set, the number of extrema and the number of zero crossings must either equal or differ at most by one; and (2) at any point, the mean value of the envelope defined by the local maxima and the envelope defined by the local minima is zero (Huang *et al.*, 1998). The intrinsic mode functions are obtained using an algorithm called sifting. First, the "zero-mean" of the data is found. This is done by taking the local maxima of the data and interpolating these points using a cubic spline interpolation, and by doing the same for the local minima of the data. The average of these two splines gives the zero-mean

of the data, and it represents the local average of the data. Subtracting this mean from the data completes one "sift". This sifting is repeated until some stopping criterion is satisfied. Once this criterion is met, the sifted data supposedly satisfies the properties of an IMF and is called the first IMF of the signal. This IMF is subtracted from the original signal and the process is applied again to the remainder of the signal, giving the second IMF. By successively subtracting out IMFs and repeating the process on the remainder of the signal, the original signal is decomposed into a set of IMFs whose sum is the original signal. Figure 7.3 illustrates the EMD applied to a set of ultrasound data.

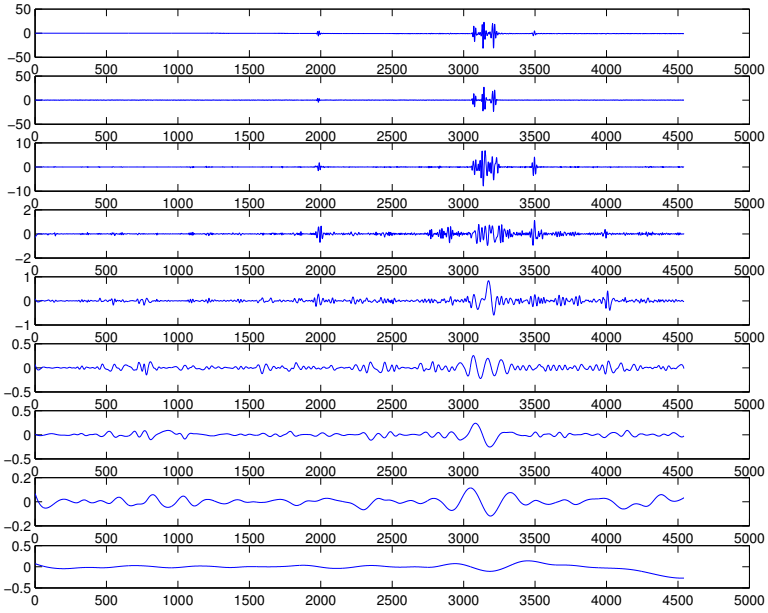

Figure 7.3. Empirical mode decomposition of one-dimensional signal. The first plot is the original data, and the successive intrinsic mode functions follow. (Note the difference in amplitude scales.) The first IMF contains the highest frequency data, while later IMFs contain lower frequency (less oscillatory) data.

2D EMD

The sample data that we used can be seen in Figure 7.4. This data is two-dimensional, consisting of one space dimension (corresponding to the set of transducers distributed in space) and one time dimension. To analyze this data, we used a two-dimensional EMD that is analogous to doing a two-dimensional Discrete Fourier Transform. The EMD is performed on each column of the data independently, producing a set of IMFs for each column. Then, the EMD is performed row-wise on each of the resulting IMFs. The final result is a rectangular "grid" of IMFs as seen in Figure 7.5, with each direction on the grid corresponding to successive IMFs in that direction, similar to how a 2D DFT gives a 2D grid of outputs with each direction corresponding to higher frequencies in that direction. Once this "grid" of IMFs is obtained, subsets of them are summed together to produce

"summed modes", whose plots are seen in Figure 7.6. The first of the plots in this figure is obtained by summing each of the images lying in the first row or column of the 2D EMD grid (Figure 7.5). The second plot is obtained by summing the remaining images that lie in the second row or column, and so on.

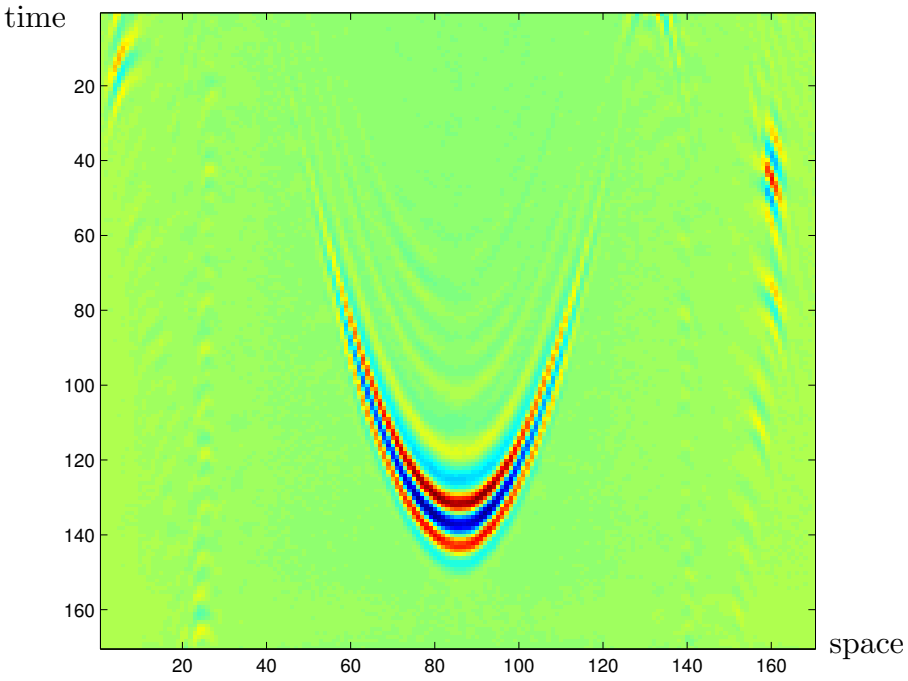

Figure 7.4. Two-dimensional data sample used.

Results

To see how the EMD method fared in isolating the desired signal from the artifacts, we took a cross-section of the data (corresponding to the data from a single transducer) and plotted the original data along with the "summed modes" from Figure 7.6. (See Figure 7.7.) Qualitatively speaking, the results look promising. By visually inspecting the first mode (green curve), we see that it contains much of the wanted part of the original signal (before 50 on the horizontal axis), but it does not contain the ringdown artifacts that occur later in the signal (after 50). We see that some of the artifacts appear in the second mode (red curve). While these preliminary results look promising, further work needs to be done to determine the viability of the EMD approach to eliminating the ringdown artifacts in the ultrasound signal. In addition, further analysis needs to be done on the IMFs in order to obtain a physical interpretation of each of the IMFs.

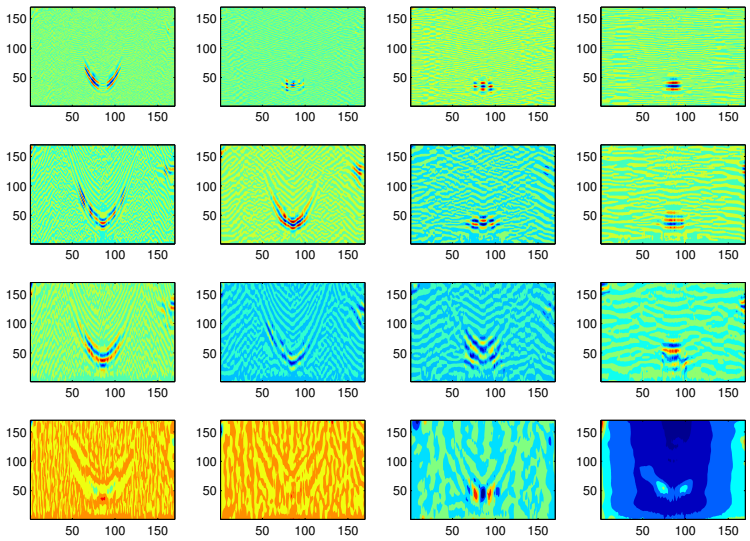

Figure 7.5. 2D EMD of the 2D data in Figure 7.2. Moving to the right corresponds to higher IMFs in the spatial axis, and moving down corresponds to higher IMFs in the time axis.

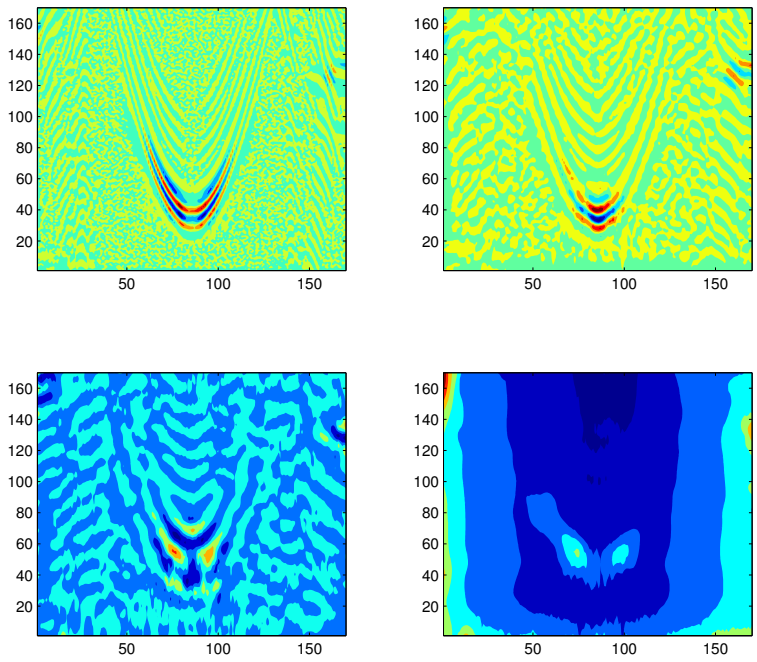

Figure 7.6. Summed modes. The top left plot is the sum of all of the images that lie in the first row or column of Figure 7.5, the top right plot is the sum of all the remaining images that lie in the second row or column, the bottom left plot is the sum of the remaining images in the third row or column, and the bottom right plot is the same as the bottom right plot of the previous figure.

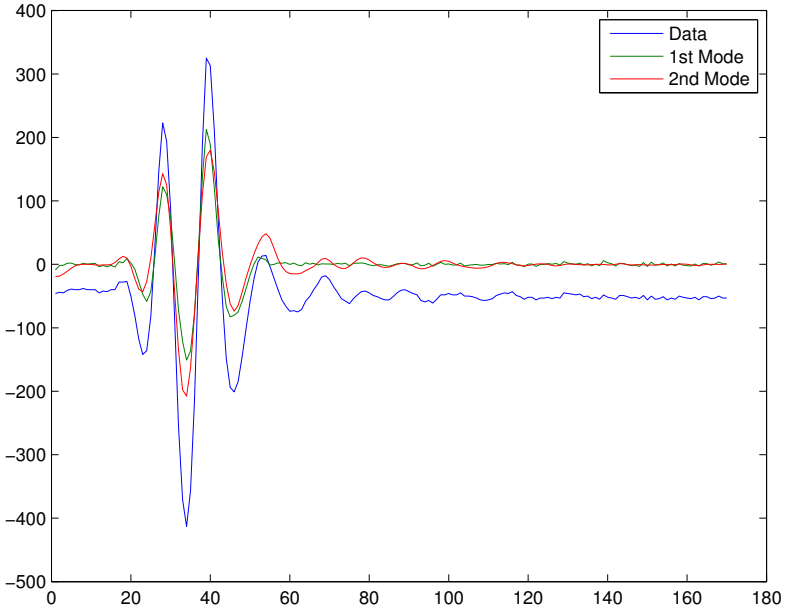

Figure 7.7. Plot of time series from a single transducer, and the first two modes obtained from Figure 7.4. The first mode (green curve) contains the desired data (data for times less than approx. 50), but the ringdown artifacts (time$>$ 50) are not present.

Section 8: Conclusions and Further Research

Internal interfaces in the impedance-matching layer of an ultrasound transducer introduce echoes into the transmitted and received signals. The purpose of our study was to develop an algorithm to reduce or filter out these echoes to improve the fidelity of images obtained from the nonlinear propagation of acoustic signals through tissue. We approached the problem from three perspectives: (1) by developing simple mathematical models of the various physical processes, (2) by numerically simulating the nonlinear propagation of the ultrasonic signal using mathematical models obtained from the literature, and (3) by extracting the echoes from the signal data using the ensemble empirical mode decomposition.

Considerable effort was invested in the forward problem, *i.e.*, modeling the origin and evolution of the echoes, in order to understand how best to remove them. The origin of the echoes was studied using a linear model that incorporated multiple reflections of pulse-like data through a single layer. The separation of scales inherent in the transducer signal was exploited to obtain an asymptotic estimate of the time-decay observed in the analytical signal, used as an approximation of the signal envelope modulating a fast carrier. This provided a plausible interpretation of the echoes as a ringing phenomenon. However, by the end of the week the group was unable to obtain a satisfactory match between the period of the experimentally measured echoes and the ringing analysis based on the linear model.

A standard model originally proposed by Westervelt was adopted to incorporate nonlinearity in the forward propagation problem. The separation of scales mentioned above motivated a multiple-scales derivation of a set of envelope equations for the signal, which can conveniently be decomposed into the fundamental frequency and its harmonics. In particular, truncating the resulting envelope equations at the second harmonic provide a simple model that can, in principle, be used to remove the second harmonic from the measured signal. Time did not allow further pursuit of this direction.

Finally, signal processing techniques applied directly to the measured data offered the most immediate success in extracting the echoes. In particular, the ensemble empirical mode decomposition appeared to capture the usable signal and its echoes in different intrinsic mode functions. This early promise is mitigated by the fact that the empirical mode decomposition is an *ad hoc* approach that lacks basic features important for rigorous analysis, such as stability and orthogonality. Nevertheless, recent attempts by Liao et al. (2010) to enhance blood-to-tissue contrast in acoustic data demonstrated that the empirical mode decomposition was somewhat effective in removing the effect of microbubbles, suggesting that the method's effectiveness as a flexible and practical tool might outweigh its mathematical limitations.

Appendix

We were told that the frequency at which the wave is sent into the medium is given by

$$f_{\mathrm{c}} = 4 \text{ MHz} = \frac{4 \times 10^6}{\mathrm{s}}, \tag{A.1}$$

which yields a typical value for ω_{c}:

$$\omega_{\mathrm{c}} = 2\pi f_{\mathrm{c}} = 2\pi \left(\frac{4 \times 10^6}{\mathrm{s}} \right) = \frac{2.51 \times 10^7 \text{ rad}}{\mathrm{s}}. \tag{A.2}$$

The sampling frequency is given by

$$f_{\mathrm{s}} = 33 \text{ MHz} = \frac{33 \times 10^6}{\mathrm{s}}, \tag{A.3}$$

from which we have

$$\frac{f_{\mathrm{s}}}{f_{\mathrm{c}}} = \frac{33}{4} = 8.25.$$

Tab. 1. Properties of transducer components.

Parameter	backing	PZT	layer 1	layer 2	fluid
thickness (μm)	190	220	120	130	
sound speed (m/s)	7000	4000	2700	2100	1500
Z (MRayles)	100	30	6.7	2.2	1.5
flight time (ms)	27	55	44	62	

Various properties of the transducer components are listed in Tab. 1. Note that $c_{\mathrm{T}} < c_1$, as expected. Since the structures we wish to image are usually centimeters below the surface, this does guarantee that $L \gg 1$, as required. In fact, other values quoted for the wavelength λ are an order of magnitude smaller:

$$1 \times 10^{-4} \text{ m} \leq \lambda \leq 5 \times 10^{-4} \text{ m}.$$

There are a few anomalies. First, if the layer width is tuned to be 1/4 of the wavelength of a certain frequency, it would seem that both should be tuned to have the same flight time.

In particular, we may use the impedance values to calculate the reflection coefficient from section 2:

$$R_{\mathrm{T}} = \frac{1.5 - 6.7}{1.5 + 6.7} = -0.63, \tag{A.4a}$$

which is in the range claimed. Similarly, the reflection coefficient from section 3 becomes

$$R_{\mathrm{P}} = \frac{30 - 6.7}{30 + 6.7} = 0.63, \tag{A.4b}$$

which is also in the range claimed. Note the similarity in the values.

To calculate a typical value of L, we work with the water tank experiment, where the steel reflector is about 1.5 cm away from the transducer. Then we have

$$L = \frac{(1.5 \times 10^{-2}\ \mathrm{m})(2.51 \times 10^{7}\ \mathrm{s}^{-1})}{2100\ \mathrm{m/s}} = 179. \tag{A.5}$$

A typical pressure wave in the transducer can be

$$p_{\mathrm{c}} = 10\ \mathrm{MPa} = 10^{7}\ \frac{\mathrm{kg}}{\mathrm{m} \cdot \mathrm{s}^{2}}. \tag{A.6}$$

The density of water can be well approximated by

$$\rho_{\mathrm{e}} = 10^{3}\ \frac{\mathrm{kg}}{\mathrm{m}^{3}}, \tag{A.7}$$

which yields a value of ϵ of

$$\epsilon = \frac{10^{7}\ \mathrm{kg}/(\mathrm{m} \cdot \mathrm{s}^{2})}{(1493\ \mathrm{m/s})^{2}(10^{3}\ \mathrm{kg/m}^{3})} = \frac{10^{-2}}{2.23} = 4.49 \times 10^{-3}, \tag{A.8}$$

which is small, as expected.

Given a value for the viscosity of water

$$\mu = 1\ \mathrm{cP} = 10^{-3}\ \mathrm{mPa} \cdot \mathrm{s} = 10^{-3}\ \frac{\mathrm{kg}}{\mathrm{m} \cdot \mathrm{s}}, \tag{A.9}$$

we may calculate η:

$$\eta = \frac{(10^{-3}\ \mathrm{kg/m} \cdot \mathrm{s})(4 \times 10^{6}\ \mathrm{s}^{-1})}{(10^{3}\ \mathrm{kg/m}^{3})(1493\ \mathrm{m/s})^{2}} = 1.8 \times 10^{-6}.$$

Nomenclature

Units are listed in terms of length (L), mass (M), or time (T). If the same letter appears both with and without tildes, the letter with a tilde has dimensions, while the letter without a tilde is dimensionless. Boldface refers to vectors. The equation number where a particular quantity first appears is listed, if appropriate.

C: matrix in discrete system.
c: wave speed, L/T (2.1).
$\mathcal{F}(\cdot)$: Fourier transform (2.25).
$G(x,t)$: Green's function (2.7).
J: maximum value of j.
j: indexing variable.
K: maximum value of k.
k: indexing variable.
M: integer characterizing m (2.19).
m: sampling variable (2.19).
n: arbitrary constant, variously defined.
$P(t)$: pressure envelope (3.1).
$\tilde{p}(\tilde{x},\tilde{t})$: pressure, M/LT^2.
q: variable in discrete system.
R: reflection coefficient (2.8).
r: inverse of speed ratio (2.5b).
$\tilde{t}$: time, T.
$\tilde{v}(\tilde{x},\tilde{t})$: velocity in the $\tilde{x}$-direction, L/T.
$\tilde{x}$: distance from PZT interface, L.
$\tilde{y}$: distance along transducer, L.
$\mathcal{Z}$: the integers.
Z: impedance, ML^2T^{-1}.
α: constant in constitutive equation (5.1), M/LT^2.
β: dimensionless constant, variously defined.
γ: dimensionless constant in constitutive equation (5.1).
ϵ: dimensionless parameter (5.3)
λ: wavelength, L.
η: pressure ratio, (5.12).
θ: traveling wave variable.
ρ: density, M/L^3.
μ: bulk viscosity, M/LT (5.12).
τ: dummy variable.
ω: frequency, T^{-1}.

Other Notation

c: as a subscript, used to indicate a characteristic value.
d: as a subscript, used to indicate delay.
e: as a subscript, used to indicate an equilibrium value.
L: as a subscript, used to indicate a matching layer (2.1).
P: as a subscript, used to indicate PZT (2.3).
R: as a subscript, used to indicate the received signal.
s: as a subscript, used to indicate sampling (2.18).
T: as a subscript, used to indicate tissue.
$\hat{}$: used to indicate the Fourier transform of a quantity (2.21).
$*$: as a subscript, used to refer to an $O(1)$ quantity.

References

Bracewell, D. *The Fourier Transform and Its Applications*, 3rd ed. Boston: McGraw-Hill, 2000.

Georgia State University, "Speed of Sound in Various Bulk Media." `http://hyperphysics.phy-astr.gsu.edu/hbase/tables/soundv.html`. Accessed June 15, 2010.

Girnyk, S., Barannik, A., Barannik, E., Tovstiak, V., Marusenko, A., and Volokhov, V., "The Estimation of Elasticity and Viscosity of Soft Tissues *in vitro* Using the Data of Remote Acoustic Palpation." *Ultrasound in Med. & Biol.*, **32** (2006), 211–219.

Huang, N., Shen, Z., Long, S., Wu, M., Shih, H., Zheng, Q., Yen, N., Tung, C., and Liu, H., "The empirical mode decomposition and the Hilbert spectrum for nonlinear and non-stationary time series analysis," *Proc. Roy. Soc. London A*, **454** (1998), 903–995.

Liao, A.-H., Shen, C.-C., and Li, P. C., "Potential Contrast Improvements in Ultrasound Pulse Inversion Imaging Using EMD and EEMD." *IEEE Trans. Ultras. Ferroelectr. Freq. Control*, **57** (2010), 317–326.

Hamilton, M. F. and Blackstock, D. T. *Nonlinear Acoustics: Theory and Applications. New York: Academic Press, 2007.*

Kammler, D. *A First Course in Fourier Analysis*, 2nd ed. New York: Cambridge University Press, 2008.

Naugolnykh, K. and Ostrovsky, L. *Nonlinear Wave Processes in Acoustics.* New York: Cambridge University Press, 1998.

Novikov, B. K., Rudenko, O. V., and Timoshenko, V. I. *Nonlinear Underwater Acoustics.* New York: American Institute of Physics, 1987.

Sub-Sea Acoustic Lab, "Sound Reflection." `http://www.sal2000.com/ds/ds3/Acoustics/Wave Reflection.htm`. Accessed June 15, 2010.